Protein Phosphatase 1 in association with Bud14 inhibits mitotic exit in *Saccharomyces cerevisiae*

Dilara Kocakaplan[1], Hüseyin Karabürk[1], Idil Kirdok[1], Şeyma Nur Erkan[1], Cansu Dilege[1], Ayse Koca Caydasi[1,*]

1. Department of Molecular Biology and Genetics, Koç University, Istanbul, Turkey

*Corresponding author

E-mail: aykoca@ku.edu.tr

Abstract

Saccharomyces cerevisiae, also known as the budding yeast, orients and elongates its mitotic spindle along its polarity axis in order to segregate one copy of its genomic DNA to the daughter cell. When accurate positioning of the mitotic spindle fails, a surveillance mechanism, named the Spindle Position Checkpoint (SPOC), prevents cells from exiting mitosis unless the spindle orientation is corrected. Such mitotic arrest provides cells time to align their spindle correctly before cell division is completed. Mutants with a defective SPOC loss their genomic integrity, become multiploid and aneuploid. Thus, SPOC is a crucial checkpoint for the budding yeast. Yet, a comprehensive understanding of how SPOC mechanism works is budmissing. In this study, we identified Bud14 as a novel checkpoint protein. We showed that the mitotic exit inhibitory function Bud14 requires its association with the type 1 protein phosphatase, Glc7. Cells bearing versions of Bud14 that cannot interact with Glc7 or a temperature sensitive mutant of Glc7 were SPOC deficient. Our data indicate that Glc7-Bud14 inhibits mitotic exit by promoting dephosphorylation of Bfa1 during anaphase and limiting the levels of Bfa1 at the spindle pole bodies. Our results support a model in which Glc7-Bud14 works parallel to the SPOC kinase Kin4 in regulating Bfa1, the most downstream effector of SPOC that inhibits mitotic exit.

Introduction

The direction along which chromosomes are segregated has consequences on the daughter cells' fate during division of cells that are polarized. Budding yeast undergoes asymmetric cell division in every cell cycle and is an intrinsically polarized cell. In every cell cycle, a new cell

buds on the mother cell and pinches of from this location at the end of the cell division, giving rise to a young daughter cell and an old mother cell. In order for the daughter cell to receive one copy of the duplicated genetic material, budding yeast has to segregate its chromosomes along the mother-to-bud polarity axis, which requires positioning of the mitotic spindle apparatus along this direction. The correct orientation of the mitotic spindle is achieved by two redundant pathways, namely the "early" and "late" pathways, which are dependent on the Adenomatous Polyposis Coli (APC) homolog Kar9 and the microtubule motor protein Dyn1 respectively (Adames and Cooper, 2000; Beach et al., 2000; Li et al., 1993; Siller and Doe, 2009).

Correct orientation of the mitotic spindle is monitored by a mitotic checkpoint named the Spindle Position Checkpoint (SPOC) in budding yeast. SPOC prevents cell cycle progression of cells that fail to orient their spindle in the mother-to-bud direction, and hence provides time for the cells to correct their spindle orientation before mitotic exit (Adames et al., 2001; Bardin et al., 2000; Bloecher et al., 2000; Pereira et al., 2000; Yeh et al., 1995). Yeast cells with defects in the spindle positioning pathways or cells with impaired microtubule function rely on the SPOC to main their ploidy. Absence of SPOC causes multinucleation, enucleation and aneuploidy in budding yeast. A SPOC like checkpoint also exists in Drosophila and may be present in higher eukaryotes (Cheng et al., 2008; O'Connell and Wang, 2000; Pereira and Yamashita, 2011).

In response to spindle mispositioning, SPOC inhibits cell cycle progression by inhibiting the Mitotic Exit Network (MEN) (Baro et al., 2017; Caydasi et al., 2010a; Caydasi and Pereira, 2012; Weiss, 2012). MEN is a GTPase driven signaling pathway that is essential for mitotic exit in budding yeast (Jaspersen et al., 1998; Shou et al., 1999). A single conserved phosphatase, named Cdc14 triggers mitotic exit in budding yeast through inactivation of the mitotic Cyclin Dependent Kinase (CDK) and dephosphorylation of CDK targets (Manzano-Lopez and Monje-Casas, 2020). At the anaphase onset, a transient wave of Cdc14 activation is triggered by the cdcFourteen Early Anaphase Release (FEAR) network; whereas later in anaphase the MEN promotes fully activation of Cdc14 (Jaspersen et al., 1998; Lee et al., 2001a; Rock and Amon, 2009; Shou et al., 1999). A Ras-like small GTPase named Tem1 is the main switch located near the top of the MEN (Lee et al., 2001a; Morishita et al., 1995; Scarfone and Piatti, 2015; Shirayama et al., 1994b). When bound to GTP, Tem1 initiates the MEN signaling by recruiting the Cdc15 kinase to the spindle pole bodies (centrosome equivalent in yeast, SPB)

which therein activates Dbf2 kinase in association with its regulatory subunit Mob1 (Asakawa et al., 2001; Cenamor et al., 1999; Visintin and Amon, 2001).

SPOC inhibits MEN through inactivation of Tem1 by a bipartite GTPase Activating Complex (GAP) composed of Bfa1 and Bub2 proteins (Geymonat et al., 2002). Activity of the Bfa1-Bub2 GAP complex is tightly regulated at the level of Bfa1 phosphorylation. In cells with a correctly positioned anaphase spindle, the polo like kinase Cdc5 phosphorylates Bfa1 to prevent Bfa1-Bub2 GAP activity towards Tem1 (Hu et al., 2001). CDK also phosphorylates Bfa1 in an activating manner until anaphase when this phosphorylation is removed in a FEAR related manner (Caydasi et al., 2017) In the presence of spindle misalignment, however, Kin4 kinase phosphorylates Bfa1 (Maekawa et al., 2007). This phosphorylation prevents inhibitory phosphorylation of Bfa1 by Cdc5 kinase (Pereira and Schiebel, 2005). Consequently, Bfa1-Bub2 GAP complex activity is promoted, Tem1 activity is prevented, and exit from mitosis is inhibited.

SPBs, serving as a scaffold, play a key role in mitotic exit and its timely regulation by the spindle position (Campbell et al., 2020; Gruneberg et al., 2000; Pereira and Schiebel, 2001; Valerio-Santiago and Monje-Casas, 2011). When the spindle is properly oriented, Bfa1-Bub2 and Tem1 reside in a preferential, asymmetrical manner at the SPB that moves to the daughter cell (dSPB) (Molk et al., 2004; Pereira et al., 2000). On contrary, Kin4 localizes exclusively to the SPB that stays in the mother cell (mSPB) during an unperturbed anaphase (D'Aquino et al., 2005; Pereira and Schiebel, 2005). Spindle misalignment alters the SPB localization of SPOC components. Upon mispositioning of the mitotic spindle, Kin4 localizes to both SPBs (Gislene Pereira & Schiebel, 2005). Phosphorylation of Bfa1 by Kin4 promotes binding of the 14-3-3 family protein Bmh1 to Bfa1 which causes dissociation of Bfa1-Bub2 from SPBs (Caydasi et al., 2012; Caydasi et al., 2014; Caydasi and Pereira, 2009). Hence, upon spindle mispositioning, the amount of Bfa1-Bub2 at both SPBs decreases, while their cytoplasmic levels increase. The release of Bfa1-Bub2 from SPBs is thought to keep Bfa1-Bub2 away from the inhibitory kinase Cdc5 and thus prevent inactivation of Bfa1-Bub2 by Cdc5. However, what dephosphorylates the Cdc5 phosphorylated Bfa1 remains elusive.

Here, we identified Bud14 as a novel SPOC protein. Deletion of *BUD14* rescued cold sensitivity of *lte1*Δ cells, lethality of mitotic exit deficient *lte1*Δ *spo12*Δ cells, and growth defect of MEN temperature sensitive mutants. Our data showed that *bud14*Δ cells accumulated multinucleated phenotypes when spindle positioning was impaired in cells via deletion of

KAR9 or *DYN1*. Fluorescence time-lapse microscopy revealed that *bud14*Δ cells progressed to mitotic exit regardless of the spindle position. We further found that the mitotic exit inhibitory function Bud14 required its association with the type 1 protein phosphatase, Glc7. A temperature sensitive version of Glc7 (Glc7-ts) and a version of Bud14 that cannot interact with Glc7 caused SPOC deficiency. Furthermore, they rescued growth of mitotic exit mutants. Mitotic exit inhibitory role of Bud14 was not through their role in formin regulation. Consequently, a Bud14 mutant that cannot bind to the formin Bnr1 was functional in terms of mitotic exit inhibition. Yeast two hybrid data indicated an interaction between Bfa1 and Bud14 that required the presence of Bub2, which suggests that Bud14 may recognize Bfa1-Bub2. We observed that, Bud14 promoted Bfa1 dephosphorylation in anaphase, as cells lacking Bud14 accumulated hyperphosphorylated Bfa1 forms during anaphase. Of importance, although Bud14 was not enriched at spindle poles, Glc7 localized to the spindle poles in cells with misaligned anaphase spindles indicating the proximity of Glc7 to Bfa1 during anaphase. Intriguingly, *bud14*Δ cells had more Bfa1, Bub2 and Tem1 localized to SPBs, especially to the daughter oriented SPB, suggestive of a role for Bud14 in limiting SPB-bound levels of Bfa1-Bub2. Our data indicated that Kin4 function was not altered in *bud14*Δ cells. In addition, we observed an additive SPOC deficiency phenotype in *kin4*Δ *bud14*Δ cells compared to *kin4*Δ or *bud14*Δ, suggesting a mitotic exit inhibitory function for Glc7-Bud14 parallel to the SPOC kinase Kin4.

Materials Methods

Yeast methods, strains and growth

All yeast strains used are isogenic with S288C and are listed in Table 1. Basic yeast methods and growth media were as described (Sherman, 1991). Carbon source is glucose unless otherwise stated. When necessary 2% D-Raffinose, 3% D(+)-Galactose was used instead of glucose. Yeast strains were grown at 30 °C and in rich medium unless otherwise stated. Plasmid containing strains were grown in SC media lacking the appropriate auxotrophic nutrients. The temperature sensitive mutants and *kar9*Δ cells were maintained at 23 °C. Cassette PCR-based gene editing method was used for chromosomal gene deletion and C-terminal or N-terminal tagging (Janke et al., 2004; Knop et al., 1999). To determine genetic interactions based on growth mutant yeast strains bearing the wildtype gene on a *URA3*-based plasmid (pRS316) were spotted on 5-Fluoroorotic acid (5FOA) plates. 5FOA plates negatively selects for the

URA3-based plasmid and allows for observation of the growth phenotype. Most *kar9*Δ cells were maintained complemented with *KAR9* on *URA3* based centromeric plasmid (pGW399), and stroke on 5FOA plates to induce plasmid lost shortly before experiments on SPOC analysis. The plasmids used in this study are listed in Table 2.

Cell growth comparison on agar plates

Yeast cultures were inoculated in appropriate growth conditions for at least 24-48 hours. The OD_{600} of the cultures were adjusted to 1 and 10-fold serial dilutions were made using sterile PBS. 10 µl of serial dilutions were spotted on appropriate agar plates and grown at appropriate temperatures for 1-3 days.

Cell cycle synchronizations

Cells were synchronised at G1 phase by treating log-phase cultures with 10 µg/ml α-factor (Sigma #T6901) dissolved in DMSO and incubating for one and a half doubling time.

For synchronization at metaphase, 15 µg/ml nocodazole (Sigma #M1404) dissolved in DMSO were added to log-phase cultures and incubated for ~2h. The arrest was confirmed by microscopy after fixing the cells with 70% Ethanol and re-suspending in PBS containing 1 µg/ml 4',6-diamino-2-phenylindole (DAPI, Sigma). For nocodazole arrest from G1 synchronized cells, cells were first treated with α-factor and released in nocodazole containing YPAD.

For telophase arrest via Tem1 depletion, Gal1-UPL-Tem1 bearing cells were grown to log-phase in Raffinose-Galactose containing medium and synchronized in G1 using α-factor in the same medium. 30 min before G1 synchronization was completed, glucose was added to the culture to give 2% final concentration. Then cells were released from α-factor in YPAD. The arrest was confirmed by microscopy after ethanol fixation of the cells and staining the nucleus with DAPI.

Protein Methods

Total yeast protein extracts and Western blotting were performed as described (Janke et al., 2004). Primary antibodies were Mouse-anti-HA (Gift from Gislene Pereira), Rabbit anti-Clb2 (Gift from Gislene Pereira) and Rabbit-anti-Tubulin (Abcam EPR13799). Secondary antibodies were Goat-anti-rabbit (Advansta #R-05062-500) or Goat-anti-mouse (Advansta #R-05071-500) horse radish peroxidase (HRP) conjugated secondary antibodies.

Microscopy Methods

All fluorescence microscopy methods were performed using Carl ZEISS Axio Observer 7 motorized inverted epifluorescence microscope equipped with Colibri 7 LED light source, Axiocam 702 Monochrome camera, 100X and 63X Plan Apochromat immersion oil objective lenses, Filter sets 95 (GFP/Cherry), 20 (Rhodamin), FITC and DAPI, and an XL incubation and climate chamber. For Kin4-GFP, GFP-Tubulin, Bud14-GFP analysis 63X objective was used. For analysis of Bfa1-GFP, Bub2-GFP and Tem1-GFP, 100X objective was used.

For time-lapse experiments, cells were prepared on glass bottom petri dishes (WVR 10810-054 Matsunami) as described (Caydasi and Pereira, 2017). Briefly, the glass center of the petri dish was covered with 6% Concanavalin A (*Canavalia ensiformis* Jack Bean, type IV Sigma C2010-G). Excess Concanavalin A was washed out and . 150 µl of culture was pipetted on the dish followed by a 30 min incubation at 30 °C. Then, cells were aspirated gently and cells there were not attached on the dish were washed out with pre-warmed fresh media. After the final wash, the dish was filled with media and taken to the microscope stage in preheated chamber 1 hour in advance the start of the time-lapse.

Still images of cells were taken from sample wet mount sandwiched in coverslip-slide. Cells were fixed using 70% Ethanol, stained with DAPI or analyzed live.

SPOC functionality assays

For end point analysis of SPOC functionality, log-phase kar9Δ cells cultured at 23°C were incubated at 30°C for 3-5 h or log-phase dyn1Δ cells cultured at 30 °C were incubated at 18 °C

overnight. Cells were fixed using 70% Ethanol, re-suspended in PBS containing 1 µg/ml DAPI and analyzed by microscopy. Cells bearing normal and misaligned nuclei, and cells with SPOC-deficient phenotypes including multinucleated cells were counted. Percentage of indicated phenotypes were plotted. For time lapse analysis of SPOC functionality, GFP-Tubulin bearing *kar9*Δ cells were imaged every minute for 90 min at 30 °C. 10 z-stacks of 0.4 µm thickness were taken at each time point. Anaphase duration of cells with correct and misaligned spindles was calculated as the time from the start of fast spindle elongation (metaphase-to-anaphase transition) until spindle breakdown (Caydasi et al., 2010b; Straight et al., 1997).

Fluorescence intensity quantifications

For signal intensity quantification of Bfa1-GFP, Bub2-GFP and Tem1-GFP, we took still images of live cells bearing *SPC42*-eqFP and mCherry-*TUB1* as a mitotic marker. Each still image was consisted of 12 z-stacks of 0.3 µm thickness. Z-stacks of the images were sum-projected, and mean fluorescence intensities were measured using Image J (NIH) software and corrected as described (Caydasi et al., 2012). Briefly, a 0.577 μm^2 (42 pixels) box was selected around the spindle pole body under inspection (ROI, region of interest) and the mean fluorescence intensity of the GFP signal was measured. Background fluorescence intensity was determined by measuring an area inside the cytoplasm of respective cell, near to the region of interest. The correction was done by subtracting the mean fluorescence intensity of the background from the mean fluorescence intensity of the ROI. Statistical results, average and standard deviation values were computed and plotted by using Prism (GraphPad, La Jolla, CA). Two-tailed t-test were applied to compare the statistical significance of the measurements.

Yeast Two Hybrid Assay

Yeast Two Hybrid analysis was performed as described (Meitinger et al., 2014). Briefly, indicated genes cloned into pMM5 (LexA-myc fusion, *HIS* autotrophy marker) and pMM6 (Gal4-HA fusion, *LEU2* autotrophy marker) were transformed into the yeast strain SGY37 that contains a chromosomally integrated LexA(op)-LacZ reporter for activation of the ß-galactosidase gene. Transformants were selected on SC-His-Leu agar plates, grown in SC-His-Leu media until stationary phase, diluted to 1 OD_{600} and 10 µl of each were spotted on SC-His-

Leu agar plates. Cells were grown for~ 48 hours and plates were overlaid with 0.4% soft-agar solution containing 0.4 mg/ml X-Gal, 0.1% SDS, 10 mM KCl and 1 mM $MgCl_2$. Blue color formation was monitored.

Results

Bud14 is a Novel Mitotic Exit Inhibitor

Lte1 is a mitotic exit activator that becomes essential for mitotic exit at cold temperatures (<16 ºC) (Shirayama et al., 1994a). Although the exact function of Lte1 in mitotic exit is not fully understood, one of the ways that Lte1 promotes mitotic exit is by preventing binding of the SPOC kinase Kin4 to the SPB that has migrated into the bud and by inhibiting its activity therein (Bertazzi et al., 2011; Falk et al., 2011). At physiological temperatures (i.e. 30 ºC) *lte1*Δ cells rely on the presence of the FEAR network to exit mitosis. Deletion of FEAR network components such as *SPO12* or *SLK19* in *lte1*Δ cells causes lethality due to failure of mitotic exit (Stegmeier et al., 2002). Lethality of the *lte1Δ spo12Δ* double mutants can be rescued by deletion of the known mitotic exit inhibitors *BFA1*, *BUB2* and *KIN4* (D'Aquino et al., 2005; Stegmeier et al., 2002). In order to identify novel mitotic exit inhibitors, we designed a genetic screen that looked for single gene deletions rescuing *lte1Δ spo12Δ* lethality. In addition to the known mitotic exit inhibitors *BFA1*, *BUB2* and *KIN4*, we identified *BUD14* as a novel gene that contributes to the mitotic arrest of *lte1Δ spo12Δ* cells (data not shown). Deletion of *BUD14* rescued lethality of *lte1Δ spo12Δ* cells (Figure 1A). Deletion of *BUD14* also rescued the cold sensitivity of *lte1Δ* cells at 18 ºC (Figure 1B). This data indicate that Bud14 is a novel inhibitor of mitotic exit.

Deletion of mitotic exit inhibitors such as *BFA1*, *BUB2* and *KIN4* also rescues growth of mitotic exit network (MEN) mutants. Thus, we next asked whether deletion of *BUD14* also promotes the growth of MEN mutants. For this, we made use of the temperature sensitive (*ts*) alleles of MEN components (Jaspersen et al., 1998). We deleted *BUD14* in several MEN-*ts* mutants and compared their growth at different temperatures. In line with its mitotic exit inhibitory role, deletion of *BUD14* promoted growth of *dbf2-2*, *cdc15-1*, *mob1-67* and *cdc5-10* mutants at 37 ºC, 35 ºC, 33 ºC and 35 ºC respectively (Figure 1C). Notably, *bud14Δ* did not rescue the growth of the *cdc14-2* mutant (Figure 1C). Cdc14 is the essential phosphatase that is activated at the very downstream of the MEN pathway. The fact that *bud14*Δ rescues the

MEN-*ts* mutants but not *cdc14-ts* suggest that Bud14 may function upstream of the MEN pathway.

***bud14*Δ cells are SPOC deficient**

The known mitotic exit inhibitors Bfa1, Bub2 and Kin4 are key components of the Spindle Position Checkpoint (SPOC), which is a surveillance mechanism that inhibits the MEN upon mispositioning of the anaphase spindle (D'Aquino et al., 2005; Hu et al., 2001). We next, investigated whether Bud14 has a role in SPOC. To assess SPOC activity in *bud14*Δ cells, we first used a *kar9*Δ background. Kar9 (homolog of the mammalian tumor suppressor Adenomatous polyposis coli, APC) is a microtubule and actin associated protein, that links the astral microtubules with the actin cables to allow for spindle positioning along the mother-to-daughter polarity axis (Miller and Rose, 1998). Deletion of *KAR9* causes frequent spindle mispositioning at 30 ^{o}C and above. These cells, however, can correct their mispositioned spindle due to the presence of another spindle positioning pathway that is dependent on the minus-end directed microtubule motor protein Dynein (Eshel et al., 1993; Li et al., 1993; Miller and Rose, 1998). Upon spindle mispositioning, cells with a functional SPOC arrest in anaphase until the spindle position is corrected; whereas SPOC deficient cells continue cell cycle progression resulting in formation of multinucleated and enucleated cells. As expected *kin4*Δ *kar9*Δ or *bfa1*Δ *kar9*Δ cultures accumulated multinucleated cells while *kar9*Δ cells did not (Figure 2A). *bud14*Δ *kar9*Δ cells also accumulated such multinucleated phenotypes, indicating that Bud14 is crucial for maintenance of ploidy in cells lacking *KAR9* (Figure 2A)

Bud14 was shown to have a role in promoting dynein/dynactin activity at the bud cortex (Knaus et al., 2005). Considering the function of Dynein in spindle positioning, we asked whether the reason of multinucleation in *bud14*Δ *kar9*Δ cells was the lack of Dynein activity which in turn would prevent re-aligning of the anaphase spindle. If this was the case, we would expect to see no significant multinucleation phenotype when the SPOC activity was assayed in a background that already lacked Dynein activity. For this we used *dyn1*Δ cells that are deleted for the dynein heavy chain. *bud14*Δ *dyn1*Δ cells exhibited remarkable multinucleation, similar to SPOC deficient *kin4*Δ *dyn1*Δ cells (Figure 2B). This data indicates that the role of Bud14 in Dynein activation does not account for the observed multinucleated phenotypes of *bud14*Δ *kar9*Δ.

Next, we analyzed the timing of mitotic exit in *bud14*Δ cells during spindle misalignment and normal alignment in a *GFP-TUB1 kar9*Δ background. *GFP-TUB1* served as a spindle marker. *kar9*Δ population has cells with misaligned spindles as well as cells with normally aligned spindles, and thus allows analysis of anaphase duration in both cases. Cells were imaged through fluorescence time-lapse microscopy for 90 minutes with 1 min time-resolution at 30 ^{o}C. Anaphase duration was calculated as the time elapsed between the start of fast spindle elongation and the spindle breakage, which are indications of anaphase onset and mitotic exit respectively. The majority of *kar9*Δ cells with misaligned spindles stayed arrested with an intact spindle during the course of the time-lapse movie, whereas *kin4*Δ *kar9*Δ cells with misaligned spindles broke their anaphase spindle (Figure 2C, *kar9*Δ red triangles vs *kar9*Δ *kin4*Δ black squares). *bud14*Δ *kar9*Δ cells with misaligned spindles also broke their spindle as an indication of their deficiency in keeping the SPOC arrest (Figure 2C, *kar9*Δ *bud14*Δ, black squares). These data altogether suggest that Bud14 is needed as a part of the SPOC mechanism to arrest the cells in mitosis upon spindle mispositioning.

Bud14 inhibits mitotic exit though its interaction with Glc7 and SH3 domain but not through its role in formin regulation

Bud14 is a regulatory subunit of the type I Protein phosphatase (PP1) Glc7 (Cullen and Sprague, 2002). Therefore, we asked whether Bud14 exerts its mitotic exit inhibitory role through Glc7. To address this question, we impaired Glc7-Bud14 function using several mutants. First, we used a mutant version of Bud14 that cannot bind Gcl7 (*bud14-F379A*) (Knaus et al., 2005) and analysed its ability to rescue *lte1*Δ cold sensitivity. Deletion of *BUD14* rescued the growth of *lte1*Δ cells at 16 ^{o}C as shown earlier (Figure 1B). Introducing wild type *BUD14* but not the *bud14-F379A* mutant into *lte1*Δ *bud14*Δ cells restored cold sensitivity of *lte1*Δ cells (Figure 3A). This data indicates that Glc7-Bud14 interaction is essential for mitotic exit inhibitory function of Bud14. In line with this notion, a temperature sensitive *GLC7* mutant *glc7-12 (glc7-ts)* (Andrews and Stark, 2000; Cheng and Chen, 2010), rescued the lethality of *lte1Δ spo12Δ* cells at its semi-permissive temperature (33 ^{o}C), but not at its permissive temperature (18 ^{o}C) (Figure 3B). These data altogether suggest that Glc7-Bud14 complex has a mitotic exit inhibitory function.

Next, we investigated functional importance of Glc7-Bud14 interaction in SPOC. Similar to *bud14*Δ cells, both *glc7-ts kar9*Δ and *bud14-F379A kar9*Δ cells accumulated multinucleated

cells (Figure 3C-D), indicating that the mitotic exit inhibitory function of Glc7-Bud14 is also crucial for SPOC function.

Bud14 contains an SH3 domain at its amino terminal (amino acids 262-318), deletion of which diminishes Bud14 bud cortex localization (Knaus et al., 2005). Similar to *bud14*Δ, *bud14-SH3*Δ caused SPOC deficiency (Figure 3E) and rescued *lte1*Δ cold sensitivity (Figure 3F). Thus, SH3 domain of Bud14 is important for Bud14 function in mitotic exit. Importantly, lack of SH3 domain also diminishes ability of Bud14 to interact with Glc7 (Knaus et al., 2005). Considering that Bud14 Glc7 interaction is necessary for this role, it is most likely due to impairment of Glc7-Bud14 interaction in the *bud14-SH3*Δ mutant that causes loss of mitotic exit inhibitory function of Bud14.

Bud14 is an inhibitor of the formin Bnr1 (Chesarone et al., 2009). It regulates actin cable formation and secretory trafficking through its formin-regulatory motif (amino acids 135-150) (Chesarone et al., 2009; Eskin et al., 2016). *bud14-5A* mutant with five alanine amino acid substitutions at the formin-regulatory motif lacks actin regulation by Bud14 (Eskin et al., 2016). Using this mutant, we addressed the contribution of actin regulatory role of Bud14 to its mitotic exit inhibitory function. Unlike *bud14-F379A* or *bud14-SH3*Δ*, bud14-5A* complemented the deletion of *BUD14* in *lte1*Δ and *kar9*Δ cell to the same level as wild type *BUD14* (Figure 3E-F). Thus, Bud14 function in SPOC is independent of its role in actin cable regulation but dependent on its association with Glc7.

Bud14 and Glc7 localization during spindle misalignment

Bud14 was shown to localize at bud tips, bud cortex and bud neck in a cell cycle dependent manner (Knaus et al., 2005). We investigated Bud14 localization during cell cycle and specifically in cells with misaligned anaphase spindles. In consistence with previous reports, *BUD14-GFP* localized to the future bud sites at the start of the cell cycle and enlarged there like a crest shape at the bud cortex as the bud grew. As the spindle elongated correctly in anaphase the bud cortex localization reduced gradually and finally disappeared as it started to accumulate at the bud neck (Figure 4A, upper cell, where start of anaphase is marked with an asterisk). Bud neck accumulation of Bud14-GFP coincided with spindle breakdown (indicated with an arrow) which marks the end of mitosis. When the anaphase spindle was misaligned, Bud14 localized to the bud tip similar to cells with a normally aligned spindle (Figure 4A,

lower cell, where start of the anaphase is marked with an asterisk). Bud14 localization at the bud cortex gradually disappeared as the cells stayed arrested in anaphase, in a way similar to cells with correctly aligned spindles. Bud14 did not localize to the bud neck when the spindle was misaligned, indicating the requirement of mitotic exit for this localization.

Glc7 was observed at the spindle poles during anaphase until cytokinesis and in the nucleus throughout the cell cycle, and at the bud neck after anaphase (Bloecher and Tatchell, 2000). We analysed Glc7-GFP localization in cells with misaligned spindles. Glc7 localized to the SPBs and to nucleus both in cells with a normally aligned anaphase spindle and in cells with a misaligned anaphase spindle (Figure 4B). We did not detect a significant change in Glc7-GFP localization in response to spindle misalignment in anaphase. Of importance, under our experimental conditions, we could not detect Bud14 localization at the SPBs, neither it was previously reported to our knowledge. Nevertheless, SPB localization of Glc7 suggests that Glc7-Bud14 may have access to SPOC machinery at the SPBs.

Bud14 interacts with Bfa1 in yeast two hybrid system

We sought to understand whether Bud14 interacts with SPOC proteins. For this, we performed a yeast two hybrid assay. We used Bfa1, Bub2 and Kin4 as a bait and Kel1 as a positive control in this assay. Formation of a blue color indicates activation of the ß-galactosidase gene and hence physical interaction of LexA DNA binding domain fused with Bud14 (PMM5-Bud14) and Gal4-Activation Domain fused with the bait protein (pMM6-Bait protein). We observed blue color formation in cells bearing pMM5-Bud14 and pMM6-Kel1 as expected due their known physical interaction. We observed a similar interaction between Bud14 and Bfa1 but not Bub2 or Kin4 (Figure 5A). Intriguingly, deletion of *BUB2* ceased blue color formation in cells with pMM5-Bud14 and pMM6-Bfa1, indicating that Bud14-Bfa1 interaction is dependent on Bub2 (Figure 5B). Although we could observe an interaction in the yeast two hybrid system we could not detect Co-IP between Bfa1-Bud14, neither we could detect an interaction between Bub2-Bud14, which may be an indication of the transient nature of Bud14-Bfa1 interaction.

Bud14 does not work in Kin4 branch of SPOC

To this end, we showed that Glc7-Bud14 has a role in mitotic exit inhibition in response to spindle mispositioning. Intriguingly, even though *BUD14* deletion caused SPOC deficiency,

duration of anaphase in *bud14*Δ *kar9*Δ cells was slightly longer during spindle misalignment than during spindle normal alignment (Figure 2C, *bud14*Δ, squares vs circles). Similar phenomenon was also observed in *kar9*Δ *kin4*Δ cells (Figure 2C, *kin4*Δ, squares vs circles) (Caydasi et al., 2017; Falk et al., 2016). This indicates that in the absence of Bud14 or Kin4, cells are still able to delay mitotic exit albeit for short time. In contrast, cells in which both *KIN4* and *BUD14* were deleted, duration of anaphase remained the same during spindle misalignment and normal alignment (Figure 2C, *kar9*Δ *bud14*Δ *kin4*Δ black squares vs circles). Thus, unlike cells lacking either Bud14 or Kin4, cells lacking both Kin4 and Bud14 cannot delay mitotic exit in response to spindle mispositioning. This data suggests that Kin4 and Bud14 work in parallel to keep the mitotic arrest in cells with misaligned spindles. In line with this notion, the percentage of multinucleated cells in *kin4*Δ *bud14*Δ *kar9*Δ was greater than that of *kin4*Δ *kar9*Δ and *bud14*Δ *kar9*Δ but was similar to the *bfa1*Δ *kar9*Δ (Figure 2A). Likewise, multinucleation phenotype was more prominent in *kin4*Δ *bud14*Δ *dyn1*Δ cells than in *kin4*Δ *dyn1*Δ and *bud14*Δ *dyn1*Δ cells (Figure 2B).

Kin4 is the key SPOC kinase that phosphorylates Bfa1 upon spindle misalignment to promote Bfa1-Bub2 GAP activity. Kin4 overexpression blocks exit from mitosis through constitutive Bfa1-Bub2 activation and thus results in lethality (D'Aquino et al., 2005). This lethality can be rescued by deletion of *BFA1* or *BUB2,* which are the most downstream SPOC components. Lethality of Kin4 overexpression can as well be rescued by deletion of *RTS1* or *ELM1*, which are Kin4 regulators and deletion of *BMH1*, which works downstream of *KIN4* (Caydasi et al., 2010b; Caydasi et al., 2014). Unlike aforementioned gene deletions, deletion of *BUD14* did not rescue the lethality of Kin4 overexpression (Figure 6A), indicating that overproduced Kin4 can still constitutively activate Bfa1 in the absence Bud14.

To further investigate the effect of Bud14 on Kin4 phosphorylation of Bfa1, we assayed Kin4 activity in cells treated with the microtubule depolymerizing drug nocodazole (Figure 6B). Nocodazole treatment promotes Kin4 phosphorylation of Bfa1 that in turn prevents Cdc5 phosphorylation of Bfa1. Consequently, Bfa1 becomes vastly hyperphosphorylated by Cdc5 in the absence of Kin4, which is not the case in *KIN4* bearing wild type cells (Maekawa et al., 2007). Such hyperphosphorylated forms of Bfa1 can be observed as slow migrating forms of Bfa1 on SDS-PAGE (Figure 6B). Like in wild type cells, Bfa1 in *bud14*Δ cells lacked the hyperphosphorylated forms of Bfa1 (Figure 6B). This data indicates that Kin4 is still able to act upon Bfa1 in the absence of Bud14. In line with this statement, Bud14 did not affect Kin4 localization or mobility shift on SDS-PAGE during the nocodazole arrest ((Figure 6C-D).

These data altogether suggest that Bud14 does not work in the Kin4 branch of SPOC, it rather acts in a pathway parallel to Kin4 to prevent mitotic exit.

Bud14 promotes Bfa1 dephosphorylation during anaphase

We next investigated whether Bud14 impinges on Bfa1phosphorylation after anaphase onset. For this, we made use of cells bearing Gal1-UPL-Tem1, which leads to a telophase arrest in glucose containing medium via Tem1 depletion. Wild type cells arrest in telophase with hyperphosphorylated Bfa1 (Bertazzi et al., 2011; Hu et al., 2001). This form of Bfa1 is established to be inactive through phosphorylation by Cdc5 (Hu et al., 2001) . *lte1*Δ cells fail to accumulate such hyperphosphorylated Bfa1 due to Kin4 localization at dSPB of *lte1*Δ cells (Figure 7A-C)). Consequently, Bfa1 hyperphosphorylation is restored in *lte1*Δ *kin4*Δ cells (Bertazzi et al., 2011) Figure 7A-C)). We asked whether *BUD14* deletion affects Bfa1 phosphorylation in *lte1*Δ cells. Remarkably, deletion of *BUD14* in *lte1*Δ cells resulted in appearance of slow migrating Bfa1 forms during anaphase (Figure 7A-C, t ≥ 75min, cells with separated nucleus ≥ %80). This form of Bfa1, however, was less abundant in *lte1*Δ *bud14*Δ than in *lte1*Δ *kin4*Δ cells (Figure 7A).

In *lte1*Δ cells, Kin4 localizes to both SPBs during anaphase (Bertazzi et al., 2011) (Figure 7D). This localization of Kin4 causes phosphorylation of Bfa1 by Kin4, which prevents Cdc5 phosphorylation of Bfa1 that appears as hyperphosphorylated forms of Bfa1 (Pereira and Schiebel, 2005). We asked whether *BUD14* deletion prevents SPB localization of Kin4 in *lte1*Δ cells, which may account for the observed Bfa1 mobility shift in *lte1*Δ *bud14*Δ. Similar to *lte1*Δ cells Kin4 localized on both SPBs in *lte1*Δ *bud14*Δ cells. Thus, we conclude that Bud14 promotes Bfa1 dephosphorylation in *lte1*Δ cells independently of Kin4 localization during anaphase.

Bud14 affects Bfa1 localization during anaphase

When the spindle is properly oriented, Bfa1-Bub2 preferentially localizes to the SPB that moves to the daughter cell (dSPB). The majority of Tem1 that is at the SPBs bind there through its association with Bfa1-Bub2, therefore Tem1 follows a similar SPB localization with Bfa1-Bub2 (Pereira et al., 2000). Of importance, Tem1 SPB localization is crucial for MEN activity.

We analyzed SPB localization of Bfa1-Bub2 and Tem1 at SPBs. For this, we first quantified the relative amounts of Bfa1-GFP at SPBs of cells with normally aligned anaphase spindles (spindle length >3µm) (Figure 8A-B). To our surprise, more Bfa1-GFP was localized to SPBs in *bud14*Δ cells (Figure 8A-B). This difference was more pronounced at the dSPB. Bub2-GFP and Tem1-GFP dSPB localization was also remarkably higher in *bud14*Δ cells compared to wild type cells (Figure 8A-B). Importantly, Increased Bfa1-GFP signal at the dSPB returned to wild type levels when *BUD14* was introduced into *bud14*Δ cells on a plasmid (Figure 8C). Increased amount of Bfa1-Bub2 and Tem1 at SPBs was also observed in mitotic cells before anaphase onset (Figure 8D).

We next asked whether SPB-bound Bfa1 levels were also higher in cells with misaligned spindles. Analysis of Bfa1-GFP intensity at SPBs of *kar9*Δ cells with misaligned anaphase spindles revealed that, *bud14*Δ *kar9*Δ cells with misoriented spindles had more Bfa1-GFP at their SPBs than *kar9*Δ cells (Figure 8E). In this case, Bfa1-GFP in *bud14*Δ cells rather resembled to Bfa1-GFP in *kin4*Δ *kar9*Δ cells (Figure 8E). However during spindle normal alignment, SPB-bound Bfa1-GFP levels in *bud14*Δ *kar9*Δ cells were higher than that in *kin4*Δ *kar9*Δ cells (Figure 8E). Indeed, in the case of spindle normal alignment Bfa1-GFP levels at the SPBs of *kin4*Δ *kar9*Δ and in *kar9*Δ cells were similar (Figure 8E). Such difference in Bfa1 localization in *kin4*Δ and *bud14*Δ cells suggests a discrepancy in these cells with respect to regulation of Bfa1 localization.

Normally, wild type cells release Bfa1 from their SPBs when the anaphase spindle elongates in the wrong direction (Caydasi and Pereira, 2009; Monje-Casas and Amon, 2009). Consequently, SPB localization of Bfa1-GFP changes from asymmetric (more at the dSPB than mSPB) to symmetric (similar at both SPBs) upon spindle mispositioning (Figure 9A). It has been shown that *kin4*Δ cells fail to release Bfa1 from their SPBs upon spindle mispositioning, which leads to increased Bfa1-GFP at the dSPB (Caydasi and Pereira, 2009) (Figure 9B). We thus asked whether *bud14*Δ cells change their Bfa1 localization from asymmetric to symmetric when the spindle starts elongating in the wrong direction. Similar to *kar9*Δ cells, *bud14*Δ *kar9*Δ cells quickly released Bfa1 from their SPBs upon elongation of the mispositioned spindle, which indicates that Kin4 is able to exerts its effect on Bfa1 in response to spindle mispositioning (Figure 9C). However, although SPB-bound levels of Bfa1 initially decreases upon spindle mispositioning, Bfa1 later accumulates at one of the SPBs (Figure 9C) which may account for the observed difference in the amount of SPB-bound Bfa1 in *bud14*Δ *kar9*Δ cells with misaligned spindles (Figure 8E). This result is in line with our previous

conclusion that Bud14 does not affect Kin4 function. These data altogether indicate that Bud14 has a function in limiting the amount of Bfa1-Bub2 and Tem1 at SPBs.

Discussion

SPOC is a surveillance mechanism that inhibits mitotic exit in response to spindle mispositioning. Protein phosphorylation and localization play a key role in SPOC. Especially the activity of Bfa1, the most downstream effector of the SPOC is tightly controlled with respect to the spindle orientation through phosphorylation by the polo like kinase Cdc5 and the mother specific kinase Kin4 in an opposing manner. Phosphorylation of Bfa1 in turn affects localization of Bfa1-Bub2 and hence the activity and the localization of the GTPase Tem1 at SPBs. Despite the knowledge on Bfa1 phosphorylating kinases, knowledge on phosphatases counteracting these kinases has been limited.

Our study identified Glc7, the budding yeast protein phosphatase 1, in association with its regulatory subunit Bud14 as a novel SPOC component that inhibits mitotic exit upon spindle mispositioning. Several lines of evidence led us to this conclusion. First, similar to other SPOC proteins, *BUD14* deletion rescued growth of several mutants impaired in mitotic exit, including the cold sensitive *lte1*Δ cells, the temperature sensitive MEN mutants (*cdc15-1*, *dbf2-2*, *cdc5-10* and *mob1-67*), and the synthetic lethal *lte1*Δ *spo12*Δ cells. Impairment of Glc7 function via a Glc7-temperature sensitive (*glc7-ts*) mutant also rescued growth lethality of *lte1*Δ *spo12*Δ cells. In addition, a Bud14 mutant that cannot bind Glc7 (*bud14-F379A*) (Knaus et al., 2005) also rescued cold sensitivity of *lte1*Δ cells. Second, similar to other SPOC proteins, *BUD14* deletion caused accumulation of multinucleated cells when spindle misalignment was induced in cells by deletion of *KAR9* or *DYN1*, implying that *bud14*Δ cells are deficient in arresting upon mispositioning of the anaphase spindle. Of importance, similar to *bud14*Δ, *glc7-ts* and the *bud14-F379A* mutants were also SPOC deficient. Bud14 was implicated in the Dynein pathway of spindle positioning (Knaus et al., 2005). However, deletion of *BUD14* caused accumulation of multinucleated phenotypes not only in *kar9*Δ but also in *dyn1*Δ backgrounds indicating that the function of Bud14 in Dynein activation is not contributing to the observed multinucleation phenotype. In line with this notion, time-lapse analysis revealed that *bud14*Δ *kar9*Δ cells exited mitosis with similar timing regardless of the spindle position. Of importance the anaphase duration of *bud14*Δ *kar9*Δ cells with normally positioned spindles was not different than that of *kar9*Δ cells. Thus, similar to other SPOC components, absence of *BUD14*

does not affect the timing of mitotic exit when the spindle is correctly positioned, but it is crucial for delaying exit from mitosis when the spindle is misoriented.

The SPOC component Bfa1 is a highly phosphorylated protein in a cell cycle dependent manner. So far, Bfa1 has been shown to be the target of kinases Cdk1, Cdc5 and Kin4 (Caydasi et al., 2017; Geymonat et al., 2003; Hu et al., 2001; Pereira and Schiebel, 2005). It is possible that other kinases may also phosphorylate Bfa1. There has been an ongoing curiosity for phosphatases that act on Bfa1. So far, Cdc14 was shown to counteract Cdk1 phosphorylation of Bfa1 (Caydasi et al., 2017) and PP2A-Cdc55 was shown to decrease Cdc5 dependent phosphorylation of Bfa1 (Baro et al., 2013). Our data that Bfa1 appears hyperphosphorylated in *lte1*Δ *bud14*Δ cells in anaphase indicate that Glc7-Bud14 promotes dephosphorylation of Bfa1 during anaphase. It should yet be investigated whether this is due to direct dephosphorylation of Bfa1 by Glc7-Bud14. We were able to observe interaction of Bfa1 and Bud14 in yeast two hybrid assays, however we were unable to observe co-immunoprecipitation of Bfa1 and Bud14 (unpublished data). This might be due to a transient interaction of Bud14 with Bfa1. Alternatively, Bud14 may exert its effect on Bfa1 through regulation of Kin4 or other proteins that regulate Bfa1 phosphorylation. Our data showed that Bud14 does not affect Kin4 localization and phosphorylation. In line with this, Kin4 overexpression still caused toxicity in *BUD14* deleted cells indicating that Kin4 is still active and prevents Cdc5 phosphorylation of Bfa1 in *bud14*Δ cells. Furthermore, time-lapse analysis of Bfa1 localization during spindle misalignment suggested that Bfa1 is being removed from SPBs of *bud14*Δ cells with misaligned spindles which is not the case in *kin4*Δ cells. Thus, Kin4 is able to phosphorylate Bfa1 in the absence of *BUD14*. These data altogether exclude the possibility that Bud14 affects Bfa1 via Kin4 and suggests a model in which Glc7-Bud14 prevents mitotic exit of cells with misaligned spindles impinging on Bfa1 in a way parallel to Kin4. In support of this model, we observed an additive decrease in anaphase duration of *kin4*Δ *bud14*Δ cells with misaligned spindles compared to the cells bearing single gene deletions of either *KIN4* or *BUD14*.

The hyperphosphorylated Bfa1 observed in anaphase arrested *lte1*Δ *bud14*Δ cells resembled those seen in *lte1*Δ *kin4*Δ. It is worth noting that the usage of *lte1*Δ cells that has Kin4 localized at both SPBs in anaphase mimics a situation similar to SPOC activation during which Kin4 localize to both SPBs to prevent hyperphosphorylation of Bfa1 by Cdc5. This function of Kin4 takes place both in anaphase and metaphase (D'Aquino et al., 2005; Pereira and Schiebel, 2005). However, unlike Kin4, the effect of Glc7-Bud14 on Bfa1 phosphorylation could only

been seen during anaphase. This discrepancy between Kin4 and Glc7-Bud14 may indicate alternative scenarios: First, Glc7-Bud14 may promote dephosphorylation of sites other than those phosphorylated by Cdc5. Second, there may be redundant mechanisms of Bfa1 dephosphorylation at Cdc5 phosphorylation sites that especially dominate in metaphase. PP2A-Cdc55 was shown to counteract Bfa1 phosphorylation and cells lacking PP2A-Cdc55 activity had hyperphosphorylated Bfa1 in metaphase arrested cells (Baro et al., 2013). Therefore, one possibility is that PP2A-Cdc55 and Glc7-Bud14 may work redundantly to dephosphorylate Cdc5 phosphorylated Bfa1.

Interestingly, Bfa1-Bud14 interaction observed in the yeast two hybrid assay required presence of Bub2. Thus, Bud14 may recognize Bfa1-Bub2 as a complex, or the interaction between Bud14 and Bfa1 may require in vivo modifications of Bfa1 that occur only when bound to Bub2. It is known that all phosphorylated forms of Bfa1 abolishes in the absence of Bub2 (Lee et al., 2001b). In addition, Bfa1 fails to localize to SPBs in the absence of Bub2 (Pereira et al., 2000). Furthermore, Bfa1 phosphorylation by Cdc5 takes place at SPBs (Maekawa et al., 2007; Pereira et al., 2000). These altogether are suggestive of a model in which Glc7-Bud14 may recognize specifically a phosphorylated form of Bfa1. We favour a speculative model where Glc7-Bud14 dephosphorylates Cdc5-phosphorylated Bfa1 specifically upon spindle misalignment. This model is also in concordance with our previous conclusion that Glc7-Bud14 works in a parallel pathway to Kin4. Removal of Cdc5 dependent phosphorylations from Bfa1 by Glc7-Bud14 and isolation of Bfa1 away from the inhibitory Cdc5 kinase activity by Kin4 would concertedly reduce the levels of Cdc5 phosphorylated Bfa1.

We observed that cells lacking *BUD14* had more Bfa1, Bub2, and Tem1 especially at their SPBs, making their localization more asymmetric. The asymmetry of Bfa1 at the SPBs was shown to be dependent on Cdc5, as in the absence of Cdc5 activity Bfa1 localized more symmetrically to the SPBs (Kim et al., 2012). Thus, presence of more Cdc5 phosphorylated Bfa1 in *bud14*Δ cells may account for increased levels of Bfa1 at the dSPB and also Bub2 and Tem1 which bind SPBs in association with Bfa1. However, it does not explain why the SPB bound levels of these proteins are also increased in cells during metaphase.

Interestingly Glc7 was shown to localize to spindle poles but not Bud14 (Bloecher and Tatchell, 2000; Knaus et al., 2005). At the moment, we are unable to comment on importance of this localization for the function of Glc7-Bud14 in SPOC. Although Glc7 localizes to the poles of cells with normally aligned anaphase spindles (Bloecher and Tatchell, 2000; Knaus et

al., 2005) as well as cells with misaligned anaphase spindles, we were unable to detect Bud14 at the poles in either condition. Bud14 accumulates at the bud tip but is also present diffusely in the cytoplasm especially of the daughter cell. Bud14 may dephosphorylate Bfa1 at these locations. The fact that Bfa1 stays hyperphosphorylated in *kin4*Δ cells in which Bfa1 stays at the SPBs also supports this notion.

Interestingly a truncated version of Bud14 that lacks the SH3 domain was also unable to inhibit mitotic exit. This truncated Bud14 is unable to bind to bud cortex and also have reduced binding to Glc7 (Knaus et al., 2005). Thus, one possible explanation is that *Bud14-SH3*Δ may fail to inhibit mitotic exit due to its reduced association with Glc7. Alternatively, bud cortex localization of Bud14 may be important for Bud14 function in mitotic exit inhibition. Glc7-Bud14 was implicated in microtubule cortex interactions. Although our observations that Bud14 bud cortex localization remains low during spindle misalignment may argue against the latter, Glc7-Bud14 function at the daughter cell cortex may be particularly important for SPOC mechanism in sensing spindle positioning defects.

How spindle alignment is sensed, and this information activates SPOC still remain unknown. Data based on Kin4 activity on Bfa1 indicates that SPOC mechanism may sense microtubule-cortex interactions (Caydasi and Pereira, 2009; Maekawa et al., 2007; Monje-Casas and Amon, 2009; Pereira and Schiebel, 2005). Due to their known function in regulating microtubule-cortex interactions, Glc7-Bud14 constitutes a great candidate for sensing of such interactions (Knaus et al., 2005). Considering that Glc7 (PP1) is a conserved phosphatase, similar mechanisms may be employed by higher eukaryotes. Future work will show whether Glc7-Bud14 may act as a sensor that translates the unattached microtubule-cortex interactions to the downstream SPOC machinery.

Acknowledgements

We are grateful to Gislene Pereira (COS, Heidelberg), Elmar Schiebel (ZMBH, Heidelberg) and Matthias Peter (ETH, Zürich) and Michael Knop (ZMBH, Heidelberg) for sharing reagents, strains and plasmids. This work was supported by EMBO installation grant no 3918, ICGEP installation grant CRP/TUR17-04_EC, TUBITAK grants 117Z232, 117C041 and 118Z979 granted to A.K.C. A.K.C was funded by MSCA Individual Fellowship, 796599 COHEMEX and is a recipient of TÜBA–GEBIP, BAGEP and National Loreal Women in Science awards.

Figure Legends

Figure 1. Bud14 deletion rescues growth of cells with impaired mitotic exit. A. *bud14*Δ cells rescue the synthetic lethality of *lte1*Δ *spo12*Δ cells. **B.** *bud14*Δ cells rescue the lethality of *lte1*Δ cells at 18 ºC. **C.** *bud14*Δ rescues lethality of MEN-ts mutants. Serial dilutions of indicated strains were spotted on indicated plates and grown at given temperatures. 5-FOA plates negatively selects for the URA3 based plasmids (pRS316 containing *LTE1* in A and B, pRS316 containing the wild type copy of the corresponding MEN mutant in C). Thus only the cells that have lost this plasmid can grow on 5-FOA plates where genetic interactions can be observed.

Figure 2. *bud14*Δ cells are SPOC deficient. A-B. End-point analysis of SPOC integrity of indicated strains in *kar9*Δ **(A)** and *dyn1*Δ **(B)** background. Cells were fixed with ethanol and stained with DAPI. Cells with normally aligned nuclei (white columns), mispositioned nuclei (grey columns) and multi nucleated cells that failed to correctly position their spindle before mitotic exit (black columns) were counted by microscopy and their percentages were plotted. Graphs are average of three independent experiments. A minimum of 100 cells were counted from each strain in each experiment. Error bars show standard deviation. **C.** Single cell analysis of SPOC integrity in indicated strains. Duration of anaphase in cells with misaligned and normally aligned spindles were calculated as explained in the text and plotted. Cartoon on the left illustrates how anaphase duration was calculated. Data points in red indicate the cells in which the spindle did not break down during the time lapse movie. In this case, plotted values are the time duration during which these cells were observed in anaphase through the time lapse movie. Consequently, the actual anaphase duration is greater than the value plotted in red. This fact is emphasized in the red part of the y-axis with addition of the ">" symbol before the y-axis values. P values calculated using students' t-test are indicated on the dot plot. n: sample size.

Figure 3. Glc7-Bud14 interaction and SH3 domain plays a role in mitotic exit inhibitory role of Bud14. A. Serial dilutions of indicated strains bearing *URA3* based empty plasmid (not indicated on figure) or *BUD14*-containing *URA3* based plasmids (*BUD14, bud14-F379A*) were spotted on indicated plates and grown at indicated temperatures **B.** Serial dilutions of indicated strains bearing the *LTE1* on URA3 based pRS316 plasmid were spotted on 5-FOA and SC-Complete (SC-C) plates and grown at indicated temperatures. 5-FOA negatively

selects for *URA3* containing plasmids, thus cells lose their pRS316-*LTE1* plasmids on 5-FOA plates and genetic interactions can be observed on this plate. **C-E.** End-point analysis of SPOC integrity of indicated strains. Cells were fixed with ethanol and stained with DAPI. Cells with normally aligned nuclei (white columns), mispositioned nuclei (grey columns) and multi nucleated cells that failed to correctly position their spindle before mitotic exit (black columns) were counted by microscopy and their percentages were plotted. Graphs are average of three independent experiments. A minimum of 100 cells were counted from each strain in each experiment. Error bars show standard deviation. **F.** Serial dilutions of indicated strains bearing *URA3* based empty plasmid (not indicated on figure) or *BUD14*- containing *URA3* based plasmids (*BUD14, bud14-SH3* or *bud14-5A*) were spotted on SC-URA and grown at indicated temperatures

Figure 4. Localization of Bud14 and Glc7 in cells with normal and misaligned anaphase spindles. A. Selected frames from time-lapse series of *BUD14-GFP mCherry-TUB1* cells. Two cells, one of which has a normally aligned spindle (outlined with orange dashed line) and the other has a misaligned anaphase spindle (outlined with yellow dashed line) are shown. Asterisk indicate the time of anaphase entry. Arrow indicates spindle breakage. **B.** Representative still images of *GLC7-GFP mCherry-TUB1* cells with a misaligned anaphase spindle (top) and a normally aligned anaphase spindle (bottom). Scale bar: 2 µm.

Figure 5. Bud14 interacts with Bfa1 in yeast two hybrid system. A-B. Cells were co-transformed with pMM6 (contains Gal4 Activation Domain) and pMM5 contains LexA DNA Binding Domain) bearing indicated genes. 10 µl of 1 OD_{600} stationary culture were spotted on SC-His-Leu plates and incubated at 30 ºC for 2 days and overlaid with soft agar containing X-Gal. Empty plasmids served as a control for any self-activation. Drops in each figure comes from the same agar plate.Blue color formation indicates interaction of Bud14 with Bfa1. Kel1 was used as a known interactor of Bud14.

Figure 6. Kin4 phosphorylation of Bfa1 is not affected in *bud14*Δ cells. A. Serial dilutions of indicated strains were spotted on Glucose containing (YPD) and Galactose containing (YP Raf/Gal) agar plates. Gal1-Kin4 overexpression is induced on Galactose containing plates. **B.** Cells arrested in G1 by alpha factor treatment (t=0) were released in alpha factor free nocodazole containing media. Samples were collected at indicated time points. Bfa1-3HA mobility shift was analyzed via western blotting using anti-HA antibodies. Arrows show hyperphosphorylated forms of Bfa1. Clb2 served as a marker for mitotic progression and

Tubulin served as loading control. Percentage of separated nuclei and the budding index was assessed by microscopy after DAPI staining and serve as a control for the metaphase arrest impinged by nocodazole. **C.** Logarithmic growing cultures bearing Kin4-GFP and Spc42-eqFP were treated with nocodazole for 2 hours and Kin4 SPB and cortex localization was analyzed by microscopy. rts1Δ cells were used as a control in which Kin4 fails to localize to SPBs and cortex. **D.** Logarithmic growing Kin4-6HA cultures bearing the indicated gene deletions were treated with nocodazole for 2 hours and Kin4 mobility shift was analyzed by western blotting. *rts1*Δ served as a control for hyperphosphorylated Kin4.

Figure 7. Bud14 affects Bfa1 phospho-regulation in anaphase. A-C. Bfa1-3HA Gal1-UPL-Tem1 containing strains were released from alpha factor imposed G1 arrest (t=0) into an alpha factor free medium supplemented with glucose to achieve Tem1 depletion and samples were collected at indicated time points. Cell cycle progression was monitored by budding index (B) and DAPI plots (C) by microscopy as well as Clb2 levels by western blotting (A). Bfa1-3HA mobility shift was analyzed via western blotting (A). A lower and a higher exposed film was shown for better visualization of the up and down shifted protein ratios. Arrows indicate hyperphosphorylated forms of Bfa1-3HA (A). Protein samples of each strain at 75, 90 and 120 minutes were also loaded side-by-side for better comparison of Bfa1 mobility (A). **D.** Logarithmic growing cultures of *KIN4-GFP SPC42-eqFP mCherry-TUB1* bearing cells were imaged live. Kin4 localization at the cortex and SPBs were analyzed in anaphase cells (spindle length >5). Images of representative cells and one representative graph out of 3 experiments was shown. A minimum of 100 cells were counted from each sample.

Figure 8. More Bfa1 localizes to SPBs in the absence of *BUD14*. A. Bfa1-GFP, Bub2-GFP and Tem1-GFP signal intensity quantifications at the SPBs of cells with normal aligned anaphase spindles were plotted. Black and grey lines in the dot plots are the mean value and standard deviation respectively. **B.** Representative images of cells used in A are shown. Scale bar: 2 µm. **C.** Bfa1-GFP signal intensities at the dSPB were ploted in *BUD14* and *bud14*Δ cells bearing empty plasmid (blue and red), as well as *bud14*Δ cells bearing a *BUD14* containing plasmid. **D.** Bfa1-GFP, Bub2-GFP and Tem1-GFP signal intensity quantifications at the SPBs of cells with metaphase spindles (~2µm length) were plotted. Black and grey lines in the dot plots are the mean value and standard deviation respectively. **E.** Bfa1- GFP signal intensity quantifications at the SPBs of indicated strains with a misaligned anaphase spindle or a normally aligned anaphase spindle. Pairwise comparisons of intensities among indicated strains were assessed using Students' t-test. p-values were shown on the graph. n: sample size.

Figure 9. Bfa1-GFP localization during spindle misalignment. Selected frames from time-lapse series of *BFA1-GFP SPC42-eqFP* bearing *kar9*Δ (A), *kar9*Δ *kin4*Δ (B) and *kar9*Δ *bud14*Δ (C) gene deletions. Cell boundaries are outlined with a dashed line. Blue arrows indicate the SPBs. Scale bar: 2 µm.

Tables

Table 1. Strains used in this study

Strain Name	Description	Reference
ESM356	*MATa ura3-52 leu2Δ1 his3Δ200 trp1Δ63*	(Pereira and Schiebel, 2001)
YPH499	*MATa ura3-52 lys2-801 ade2-101 trp1Δ63 his3Δ200 leu2Δ1*	(Sikorski and Hieter, 1989)
SGY37-VIII,3	*MATa leu2 his3 trp1 ADE2 ura3-52::URA3-lexA-op-LacZ*	(Geissler et al., 1996)
GPY491	*YPH499 cdc14-2 pRS316- CDC14*	(Caydasi et al., 2017)
ESM2285	*YPH499 mob1-67 pRS316-MOB1*	(Caydasi et al., 2017)
JOY79	*YPH499 cdc5-10 pRS316-CDC5*	(Caydasi et al., 2017)
ESM2283	*YPH499 dbf2-2 pRS316-DBF2*	(Caydasi et al., 2017)
ESM2282	*YPH499 cdc15-1 pRS316-CDC15*	(Caydasi et al., 2017)
FAY145	*MATa ura3-52 his3Δ200 leu2Δ1 lte1Δ::kanMX6 pRS316-LTE1*	(Bertazzi et al., 2011)
AKY2526	*FAY145 lte1Δ::kanMX6 pRS316-LTE1 spo12Δ::natNT2*	(Caydasi et al., 2017)
AKY2916	*FAY145 lte1Δ::kanMX6 pRS316-LTE1 spo12Δ::natNT2 bud14Δ::HIS3MX6*	This study
DKY069	*FAY145 lte1Δ::kanMX6 pRS316-LTE1 bud14Δ::HIS3MX6*	This study
DKY057	*YPH499 cdc14-2 pRS316-CDC14 bud14Δ::klTRP3*	This study
DKY058	*YPH499 mob1-67 pRS316-MOB1 bud14Δ::klTRP3*	This study
DKY060	*YPH499 dbf2-2 pRS316-DBF2 bud14Δ::klTRP3*	This study
DKY061	*YPH499 cdc15-1 pRS316-CDC15 bud14Δ::klTRP3*	This study
AKY260	*ESM356 kar9Δ::HIS3MX6 pRS316-KAR9*	(Caydasi et al., 2017)
AKY315	*ESM356 kar9Δ::HIS3MX6 pRS316-KAR9 bfa1Δ::klTRP1*	(Caydasi et al., 2017)
AKY321	*ESM356 kar9Δ::HIS3MX6 pRS316-KAR9 kin4Δ::klTRP1*	(Caydasi et al., 2017)
AKY2917	*YPH499 GFP-Tub1-URA3 dyn1Δ::klTRP1 bud14Δ::HIS3MX6*	This study
AKY2918	*YPH499 GFP-Tub1-URA3 dyn1Δ::klTRP1 kin4Δ::hphNT1 bud14Δ::HIS3MX6*	This study

SHM562	*YPH499 GFP-Tub1-URA3 dyn1Δ::klTRP1*	(Pereira and Schiebel, 2005)
ESM2156	*YPH499 GFP-Tub1-URA3 dyn1Δ::klTRP1 kin4Δ::hphNT1*	(Pereira and Schiebel, 2005)
AKY346	*YPH499 kar9Δ::klTRP1 pRS316-KAR9 GFP-Tub1-ADE2*	(Caydasi et al., 2010b)
AKY351	*YPH499 kar9Δ::klTRP1 pRS316-KAR9 kin4Δ::HIS3MX6 GFP-Tub1-ADE2*	(Caydasi et al., 2010b)
SEY032	*YPH499 kar9Δ::klTRP1 pRS316-KAR9 GFP-Tub1-ADE2 bud14Δ::HIS3MX6*	This study
AKY4068	*YPH499 kar9Δ::klTRP1 pRS316-KAR9 GFP-Tub1-ADE2 bud14Δ::HIS3MX6 kin4Δ::hphNT1*	This study
DKY131	*FAY145 lte1Δ::kanMX6 pRS316-LTE1 bud14Δ::HIS3MX6 GFP BUD14 CEN URA*	This study
DKY132	*ESM356 bud14Δ::klTRP GFP BUD14 CEN URA*	This study
DKY135	*FAY145 lte1Δ::kanMX6 pRS316-LTE1 bud14Δ::HIS3MX6 pRS416-ADH-BUD14*	This study
DKY137	*FAY145 lte1Δ::kanMX6 pRS316-LTE1 bud14Δ::HIS3MX6 pRS416-ADH-BUD14 [F379A]*	This study
PAY704	*W303 MATa ade2-1 his3-11,15 leu2-3,112 ura3-1 can1-100 ssd1-d2 glc7::LEU2 trp1-1::GLC7::TRP1*	(Andrews & Stark, 2000)
PAY701	*W303 MATa ade2-1 his3-11,15 leu2-3,112 ura3-1 can1-100 ssd1-d2 glc7::LEU2 trp1-1::glc7-12::TRP1*	(Andrews & Stark, 2000)
DKY074	*PAY701 glc7::LEU2 trp1-1::glc7-12::TRP1 lte1Δ::HIS3MX6*	This study
DKY075	*PAY704 glc7::LEU2 trp1-1::GLC7::TRP1 lte1Δ::HIS3MX6*	This study
DKY078	*PAY704 glc7::LEU2 trp1-1::GLC7::TRP1 lte1Δ::HIS3MX6 pRS316-LTE1*	This study
DKY079	*PAY701 glc7::LEU2 trp1-1::glc7-12::TRP1 lte1Δ::HIS3MX6 pRS316-LTE1*	This study
DKY080	*PAY701 glc7::LEU2 trp1-1::glc7-12::TRP1 lte1Δ::HIS3MX6 pRS316-LTE1 spo12Δ::hphNT1*	This study
DKY145	*ESM356 kar9Δ::HIS3MX6 bud14Δ::klTRP1 pRS316*	This study
DKY147	*ESM356 kar9Δ::HIS3MX6 bud14Δ::klTRP1 pRS416-ADH-BUD14*	This study
DKY149	*ESM356 kar9Δ::HIS3MX6 bud14Δ::klTRP1 pRS416-ADH-BUD14 [F379A]*	This study

AKY4070	*ESM356 Spc42-eqFP611-kanMX6 GFP-BUD14 - HIS3MX6 mCherry-TUB1-URA3 kar9Δ::klTRP1*	This study
DKY197	*ESM356 Spc42-eqFP611-kanMX6 GFP- GLC7-klTRP1 mCherry-TUB1-LEU2*	This study
AKY4001	*ESM356 leu2::LEU2-pGal1-KIN4 bud14Δ::klTRP1*	This study
DKY055	*ESM356 Spc42-eqFP611-kanMX6 natNT2-Gal1-GFP-KIN4 ura3::pMET25-KIN4*	This study
UJY013	*ESM356 Spc42-eqFP611-kanMX6 natNT2-Gal1-GFP-KIN4 ura3::pMET25-KIN4 bfa1Δ::klTRP1.*	(Caydasi et al., 2010b)
AKY887	*ESM356 BFA1-3HA-hphNT1 kin4Δ::HIS3MX6*	(Caydasi et al., 2010b)
BKY091	*ESM356 BFA1-3HA-hphNT1*	(Caydasi et al., 2010b)
DGY002	*ESM356 BFA1-3HA-hphNT1 kin4Δ::HIS3MX6 bud14Δ::klTRP1*	This study
DGY003	*ESM356 BFA1-3HA-hphNT1 bud14Δ::klTRP1*	This study
GPY1033	*ESM356-1 KIN4-GFP-his3MX6 Spc42-eqFP-natNT2*	(Pereira and Schiebel, 2005)
DGY004	*ESM356 KIN4-GFP-HIS3MX6 Spc42-eqFP-natNT2 bud14Δ::klTRP1*	This study
DKY063	*ESM356 KIN4-GFP-HIS3MX6 Spc42-eqFP611-natNT2 bud14Δ::klTRP1*	This study
AKY404	*ESM356 KIN4-GFP-HIS3MX6 Spc42-eqFP-natNT2 rts1Δ::klTRP1*	(Caydasi et al., 2010b)
ESM2326	*ESM356 KIN4-6HA-hphNT1*	(Caydasi et al., 2010b)
AKY415	*ESM356 KIN4-6HA-hphNT1 rts1Δ::klTRP1*	(Caydasi et al., 2010b)
DGY001	*ESM356 KIN4-6HA-hphNT1 bud14Δ::klTRP1*	This study
DKY118	*ESM356 GAL1-UPL-TEM1::klTRP1 BFA1-3HA-hphNT1 lte1Δ::natNT2*	This study
DKY125	*ESM356 GAL1-UPL-TEM1::klTRP1 BFA1-3HA-hphNT1 kin4Δ::natNT2 bud14Δ::HIS3MX6*	This study
DKY126	*ESM356 GAL1-UPL-TEM1::klTRP1 BFA1-3HA-hphNT1 lte1Δ::natNT2 bud14Δ::HIS3MX6*	This study
DKY167	*ESM356 KIN4-GFP-HIS3MX6 Spc42-eqFP-natNT2 bud14Δ::klTRP1 lte1Δ::hphNT1*	This study
AKY038	*ESM356 Bfa1-GFP-kanMX6 Spc42-eqFP- hphNT1 mCherry-Tub1-URA3*	This study
AKY4011	*ESM356 Bfa1-GFP-kanMX6 Spc42-eqFP-hphNT1 bud14Δ::klTRP1 mCherry-Tub1-URA3*	This study

AKY4007	*ESM356 Bub2-GFP-kanMX6 Spc42-eqFP-hphNT1 mCherry-Tub1-URA3*	This study
AKY4009	*ESM356 Bub2-GFP-kanMX6 Spc42-eqFP-hphNT1 bud14Δ::klTRP1 mCherry-Tub1-URA3*	This study
AKY4013	*ESM356 Tem1-GFP-kanMX6 Spc42-eqFP-hphNT1 mCherry-Tub1-URA3*	This study
AKY4008	*ESM356 Tem1-GFP-kanMX6 Spc42-eqFP-hphNT1 bud14Δ::HIS3MX6 mCherry-Tub1-URA3*	This study
HKY114	*ESM356 Bfa1-GFP-kanMX6 Spc42-eqFP-hphNT1 mCherry-Tub1-LEU2 pRS416*	This study
HKY115	*ESM356 Bfa1-GFP-kanMX6 Spc42-eqFP-hphNT1 bud14Δ::klTRP1 mCherry-Tub1-LEU2 pRS416*	This study
HKY116	*ESM356 Bfa1-GFP-kanMX6 Spc42-eqFP-hphNT1 bud14Δ::klTRP1 mCherry-Tub1-LEU2 pRS416-BUD14*	This study
AKY043	*ESM356 BFA1-GFP-kanMX6 Spc42-eqFP-hphNT1 kar9Δ::klTRP1 pRS316-KAR9*	(Caydasi and Pereira, 2009)
BKY032	*ESM356 BFA1-GFP-kanMX6 Spc42-eqFP hphNT1 kar9Δ::klTRP1 pRS316-KAR9 kin4Δ::HIS3MX6*	(Caydasi and Pereira, 2009)
DKY081	*ESM356 BFA1-GFP-kanMX6 Spc42-eqFP hphNT1 kar9Δ::klTRP1 pRS316-KAR9 bud14Δ::HIS3MX6*	This study

Table 2. Plasmids used in this study

Plasmid Name	**Description**	**Reference**
pRS316	*URA3-dependent CEN-based yeast-E.coli shuffle plasmid. AmpR.*	(Sikorski & Hieter, 1989)
pWS103-1	*pRS304-Gal1-UPL-TEM1*	(Shou et al., 1999)
pMK60	*pRS416-endogenous BUD14-promoter- GFP-BUD14*	(Knaus et al., 2005)
pMK125	*pRS416 ADH-BUD14*	(Knaus et al., 2005)
pMK131	*pRS416 ADH-BUD14*^{F379A}	(Knaus et al., 2005)
pSM903-4	*pRS316-LTE1*	(Hofken, 2002)
pGW399-1	*pRS316-KAR9*	(Hofken, 2002)
pDKY001	*pRS416-endogenous BUD14-promoter- GFP-BUD14*$^{5A\ (135A\ 137A\ 138A\ 139A\ 140A)}$	This Study

pDKY003	*pRS416-endogenous BUD14-promoter- GFP-BUD14*$^{\Delta SH3(\Delta aa\ 262–318)}$	This Study
pMM5	p423-Gal1-lexA-Myc	(Geissler et al., 1996)
pMM6	p425-Gal1-Gal4-HA.	(Geissler et al., 1996)
pHA69-1	*pMM5-BUD14*	Gift from G. Pereira
pHA132-2	*pMM6-KIN4*	Gift from G. Pereira
pCL2-1	*pMM6-BUB2*	(Hofken and Schiebel, 2004)
pHA70-1	*pMM6-BUD14*	Gift from G. Pereira
pCL4a-3	*pMM6-BFA1*	(Hofken and Schiebel, 2004)
pTH221	*pMM6-KEL1.*	(Hofken and Schiebel, 2004)
pAFS125	*GFP-TUB1-URA3* containing integration plasmid.	(Straight et al., 1997)
pBK067-1	pRS305ΔKpnI-mCherry-*TUB1*.	(Caydasi et al., 2014)
pGW399	pRS316-*KAR9*	(Caydasi et al., 2010b)

References

Adames, N.R., and Cooper, J.A. (2000). Microtubule interactions with the cell cortex causing nuclear movements in Saccharomyces cerevisiae. J Cell Biol *149*, 863-874.

Adames, N.R., Oberle, J.R., and Cooper, J.A. (2001). The surveillance mechanism of the spindle position checkpoint in yeast. J Cell Biol *153*, 159-168.

Andrews, P.D., and Stark, M.J. (2000). Type 1 protein phosphatase is required for maintenance of cell wall integrity, morphogenesis and cell cycle progression in Saccharomyces cerevisiae. Journal of cell science *113 (Pt 3)*, 507-520.

Asakawa, K., Yoshida, S., Otake, F., and Toh-e, A. (2001). A novel functional domain of Cdc15 kinase is required for its interaction with Tem1 GTPase in Saccharomyces cerevisiae. Genetics *157*, 1437-1450.

Bardin, A.J., Visintin, R., and Amon, A. (2000). A mechanism for coupling exit from mitosis to partitioning of the nucleus. Cell *102*, 21-31.

Baro, B., Queralt, E., and Monje-Casas, F. (2017). Regulation of Mitotic Exit in Saccharomyces cerevisiae. Methods in molecular biology *1505*, 3-17.

Baro, B., Rodriguez-Rodriguez, J.A., Calabria, I., Hernaez, M.L., Gil, C., and Queralt, E. (2013). Dual Regulation of the mitotic exit network (MEN) by PP2A-Cdc55 phosphatase. PLoS genetics *9*, e1003966.

Beach, D.L., Thibodeaux, J., Maddox, P., Yeh, E., and Bloom, K. (2000). The role of the proteins Kar9 and Myo2 in orienting the mitotic spindle of budding yeast. Curr Biol *10*, 1497-1506.

Bertazzi, D.T., Kurtulmus, B., and Pereira, G. (2011). The cortical protein Lte1 promotes mitotic exit by inhibiting the spindle position checkpoint kinase Kin4. J Cell Biol *193*, 1033-1048.

Bloecher, A., and Tatchell, K. (2000). Dynamic localization of protein phosphatase type 1 in the mitotic cell cycle of Saccharomyces cerevisiae. J Cell Biol *149*, 125-140.

Bloecher, A., Venturi, G.M., and Tatchell, K. (2000). Anaphase spindle position is monitored by the BUB2 checkpoint. Nat Cell Biol *2*, 556-558.

Campbell, I.W., Zhou, X., and Amon, A. (2020). Spindle pole bodies function as signal amplifiers in the Mitotic Exit Network. Molecular biology of the cell *31*, 906-916.

Caydasi, A.K., Ibrahim, B., and Pereira, G. (2010a). Monitoring spindle orientation: Spindle position checkpoint in charge. Cell division *5*, 28.

Caydasi, A.K., Khmelinskii, A., Duenas-Sanchez, R., Kurtulmus, B., Knop, M., and Pereira, G. (2017). Temporal and compartment-specific signals coordinate mitotic exit with spindle position. Nature communications *8*, 14129.

Caydasi, A.K., Kurtulmus, B., Orrico, M.I., Hofmann, A., Ibrahim, B., and Pereira, G. (2010b). Elm1 kinase activates the spindle position checkpoint kinase Kin4. J Cell Biol *190*, 975-989.

Caydasi, A.K., Lohel, M., Grunert, G., Dittrich, P., Pereira, G., and Ibrahim, B. (2012). A dynamical model of the spindle position checkpoint. Molecular systems biology *8*, 582.

Caydasi, A.K., Micoogullari, Y., Kurtulmus, B., Palani, S., and Pereira, G. (2014). The 14-3-3 protein Bmh1 functions in the spindle position checkpoint by breaking Bfa1 asymmetry at yeast centrosomes. Molecular biology of the cell *25*, 2143-2151.

Caydasi, A.K., and Pereira, G. (2009). Spindle alignment regulates the dynamic association of checkpoint proteins with yeast spindle pole bodies. Dev Cell *16*, 146-156.

Caydasi, A.K., and Pereira, G. (2012). SPOC alert--when chromosomes get the wrong direction. Experimental cell research *318*, 1421-1427.

Caydasi, A.K., and Pereira, G. (2017). Evaluation of the Dynamicity of Mitotic Exit Network and Spindle Position Checkpoint Components on Spindle Pole Bodies by Fluorescence Recovery After Photobleaching (FRAP). Methods in molecular biology *1505*, 167-182.

Cenamor, R., Jimenez, J., Cid, V.J., Nombela, C., and Sanchez, M. (1999). The budding yeast Cdc15 localizes to the spindle pole body in a cell-cycle-dependent manner. Mol Cell Biol Res Commun *2*, 178-184.

Cheng, J., Turkel, N., Hemati, N., Fuller, M.T., Hunt, A.J., and Yamashita, Y.M. (2008). Centrosome misorientation reduces stem cell division during ageing. Nature *456*, 599-604.

Cheng, Y.L., and Chen, R.H. (2010). The AAA-ATPase Cdc48 and cofactor Shp1 promote chromosome bi-orientation by balancing Aurora B activity. Journal of cell science *123*, 2025-2034.

Chesarone, M., Gould, C.J., Moseley, J.B., and Goode, B.L. (2009). Displacement of formins from growing barbed ends by bud14 is critical for actin cable architecture and function. Dev Cell *16*, 292-302.

Cullen, P.J., and Sprague, G.F., Jr. (2002). The Glc7p-interacting protein Bud14p attenuates polarized growth, pheromone response, and filamentous growth in Saccharomyces cerevisiae. Eukaryot Cell *1*, 884-894.

D'Aquino, K.E., Monje-Casas, F., Paulson, J., Reiser, V., Charles, G.M., Lai, L., Shokat, K.M., and Amon, A. (2005). The protein kinase Kin4 inhibits exit from mitosis in response to spindle position defects. Mol Cell *19*, 223-234.

Eshel, D., Urrestarazu, L.A., Vissers, S., Jauniaux, J.C., van Vliet-Reedijk, J.C., Planta, R.J., and Gibbons, I.R. (1993). Cytoplasmic dynein is required for normal nuclear segregation in yeast. Proc Natl Acad Sci U S A *90*, 11172-11176.

Eskin, J.A., Rankova, A., Johnston, A.B., Alioto, S.L., and Goode, B.L. (2016). Common formin-regulating sequences in Smy1 and Bud14 are required for the control of actin cable assembly in vivo. Molecular biology of the cell *27*, 828-837.

Falk, J.E., Chan, L.Y., and Amon, A. (2011). Lte1 promotes mitotic exit by controlling the localization of the spindle position checkpoint kinase Kin4. Proc Natl Acad Sci U S A *108*, 12584-12590.

Falk, J.E., Tsuchiya, D., Verdaasdonk, J., Lacefield, S., Bloom, K., and Amon, A. (2016). Spatial signals link exit from mitosis to spindle position. eLife *5*.

Geissler, S., Pereira, G., Spang, A., Knop, M., Soues, S., Kilmartin, J., and Schiebel, E. (1996). The spindle pole body component Spc98p interacts with the gamma-tubulin-like Tub4p of Saccharomyces cerevisiae at the sites of microtubule attachment. The EMBO journal *15*, 3899-3911.

Geymonat, M., Spanos, A., Smith, S.J., Wheatley, E., Rittinger, K., Johnston, L.H., and Sedgwick, S.G. (2002). Control of mitotic exit in budding yeast. In vitro regulation of Tem1 GTPase by Bub2 and Bfa1. J Biol Chem *277*, 28439-28445.

Geymonat, M., Spanos, A., Walker, P.A., Johnston, L.H., and Sedgwick, S.G. (2003). In vitro regulation of budding yeast Bfa1/Bub2 GAP activity by Cdc5. J Biol Chem *278*, 14591-14594.

Gruneberg, U., Campbell, K., Simpson, C., Grindlay, J., and Schiebel, E. (2000). Nud1p links astral microtubule organization and the control of exit from mitosis. The EMBO journal *19*, 6475-6488.

Hofken, T., and Schiebel, E. (2004). Novel regulation of mitotic exit by the Cdc42 effectors Gic1 and Gic2. J Cell Biol *164*, 219-231.

Hu, F., Wang, Y., Liu, D., Li, Y., Qin, J., and Elledge, S.J. (2001). Regulation of the Bub2/Bfa1 GAP complex by Cdc5 and cell cycle checkpoints. Cell *107*, 655-665.

Janke, C., Magiera, M.M., Rathfelder, N., Taxis, C., Reber, S., Maekawa, H., Moreno-Borchart, A., Doenges, G., Schwob, E., Schiebel, E.*, et al.* (2004). A versatile toolbox for PCR-based tagging of yeast genes: new fluorescent proteins, more markers and promoter substitution cassettes. Yeast *21*, 947-962.

Jaspersen, S.L., Charles, J.F., Tinker-Kulberg, R.L., and Morgan, D.O. (1998). A late mitotic regulatory network controlling cyclin destruction in Saccharomyces cerevisiae. Molecular biology of the cell *9*, 2803-2817.

Kim, J., Luo, G., Bahk, Y.Y., and Song, K. (2012). Cdc5-dependent asymmetric localization of bfa1 fine-tunes timely mitotic exit. PLoS genetics *8*, e1002450.

Knaus, M., Cameroni, E., Pedruzzi, I., Tatchell, K., De Virgilio, C., and Peter, M. (2005). The Bud14p-Glc7p complex functions as a cortical regulator of dynein in budding yeast. The EMBO journal *24*, 3000-3011.

Knop, M., Siegers, K., Pereira, G., Zachariae, W., Winsor, B., Nasmyth, K., and Schiebel, E. (1999). Epitope tagging of yeast genes using a PCR-based strategy: more tags and improved practical routines. Yeast *15*, 963-972.

Lee, S.E., Frenz, L.M., Wells, N.J., Johnson, A.L., and Johnston, L.H. (2001a). Order of function of the budding-yeast mitotic exit-network proteins Tem1, Cdc15, Mob1, Dbf2, and Cdc5. Curr Biol *11*, 784-788.

Lee, S.E., Jensen, S., Frenz, L.M., Johnson, A.L., Fesquet, D., and Johnston, L.H. (2001b). The Bub2-dependent mitotic pathway in yeast acts every cell cycle and regulates cytokinesis. Journal of cell science *114*, 2345-2354.

Li, Y.Y., Yeh, E., Hays, T., and Bloom, K. (1993). Disruption of mitotic spindle orientation in a yeast dynein mutant. Proc Natl Acad Sci U S A *90*, 10096-10100.

Maekawa, H., Priest, C., Lechner, J., Pereira, G., and Schiebel, E. (2007). The yeast centrosome translates the positional information of the anaphase spindle into a cell cycle signal. J Cell Biol *179*, 423-436.

Manzano-Lopez, J., and Monje-Casas, F. (2020). The Multiple Roles of the Cdc14 Phosphatase in Cell Cycle Control. Int J Mol Sci *21*.

Meitinger, F., Khmelinskii, A., Morlot, S., Kurtulmus, B., Palani, S., Andres-Pons, A., Hub, B., Knop, M., Charvin, G., and Pereira, G. (2014). A memory system of negative polarity cues prevents replicative aging. Cell *159*, 1056-1069.

Miller, R.K., and Rose, M.D. (1998). Kar9p is a novel cortical protein required for cytoplasmic microtubule orientation in yeast. J Cell Biol *140*, 377-390.

Molk, J.N., Schuyler, S.C., Liu, J.Y., Evans, J.G., Salmon, E.D., Pellman, D., and Bloom, K. (2004). The differential roles of budding yeast Tem1p, Cdc15p, and Bub2p protein dynamics in mitotic exit. Molecular biology of the cell *15*, 1519-1532.

Monje-Casas, F., and Amon, A. (2009). Cell polarity determinants establish asymmetry in MEN signaling. Dev Cell *16*, 132-145.

Morishita, T., Mitsuzawa, H., Nakafuku, M., Nakamura, S., Hattori, S., and Anraku, Y. (1995). Requirement of Saccharomyces cerevisiae Ras for completion of mitosis. Science *270*, 1213-1215.

O'Connell, C.B., and Wang, Y.L. (2000). Mammalian spindle orientation and position respond to changes in cell shape in a dynein-dependent fashion. Molecular biology of the cell *11*, 1765-1774.

Pereira, G., Hofken, T., Grindlay, J., Manson, C., and Schiebel, E. (2000). The Bub2p spindle checkpoint links nuclear migration with mitotic exit. Mol Cell *6*, 1-10.

Pereira, G., and Schiebel, E. (2001). The role of the yeast spindle pole body and the mammalian centrosome in regulating late mitotic events. Curr Opin Cell Biol *13*, 762-769.

Pereira, G., and Schiebel, E. (2005). Kin4 kinase delays mitotic exit in response to spindle alignment defects. Mol Cell *19*, 209-221.

Pereira, G., and Yamashita, Y.M. (2011). Fly meets yeast: checking the correct orientation of cell division. Trends Cell Biol.

Rock, J.M., and Amon, A. (2009). The FEAR network. Curr Biol *19*, R1063-1068.

Scarfone, I., and Piatti, S. (2015). Coupling spindle position with mitotic exit in budding yeast: The multifaceted role of the small GTPase Tem1. Small GTPases *6*, 196-201.

Sherman, F. (1991). Getting started with yeast. Methods Enzymol *194*, 3-21.

Shirayama, M., Matsui, Y., Tanaka, K., and Toh-e, A. (1994a). Isolation of a CDC25 family gene, MSI2/LTE1, as a multicopy suppressor of ira1. Yeast *10*, 451-461.

Shirayama, M., Matsui, Y., and Toh, E.A. (1994b). The yeast TEM1 gene, which encodes a GTP-binding protein, is involved in termination of M phase. Mol Cell Biol *14*, 7476-7482.

Shou, W., Seol, J.H., Shevchenko, A., Baskerville, C., Moazed, D., Chen, Z.W., Jang, J., Charbonneau, H., and Deshaies, R.J. (1999). Exit from mitosis is triggered by Tem1-dependent release of the protein phosphatase Cdc14 from nucleolar RENT complex. Cell *97*, 233-244.

Sikorski, R.S., and Hieter, P. (1989). A system of shuttle vectors and yeast host strains designed for efficient manipulation of DNA in Saccharomyces cerevisiae. Genetics *122*, 19-27.

Siller, K.H., and Doe, C.Q. (2009). Spindle orientation during asymmetric cell division. Nat Cell Biol *11*, 365-374.

Stegmeier, F., Visintin, R., and Amon, A. (2002). Separase, polo kinase, the kinetochore protein Slk19, and Spo12 function in a network that controls Cdc14 localization during early anaphase. Cell *108*, 207-220.

Straight, A.F., Marshall, W.F., Sedat, J.W., and Murray, A.W. (1997). Mitosis in living budding yeast: anaphase A but no metaphase plate. Science *277*, 574-578.

Valerio-Santiago, M., and Monje-Casas, F. (2011). Tem1 localization to the spindle pole bodies is essential for mitotic exit and impairs spindle checkpoint function. J Cell Biol *192*, 599-614.

Visintin, R., and Amon, A. (2001). Regulation of the mitotic exit protein kinases Cdc15 and Dbf2. Molecular biology of the cell *12*, 2961-2974.

Weiss, E.L. (2012). Mitotic Exit and Separation of Mother and Daughter Cells. Genetics *192*, 1165-1202.

Yeh, E., Skibbens, R.V., Cheng, J.W., Salmon, E.D., and Bloom, K. (1995). Spindle dynamics and cell cycle regulation of dynein in the budding yeast, Saccharomyces cerevisiae. J Cell Biol *130*, 687-700.

Figure 1

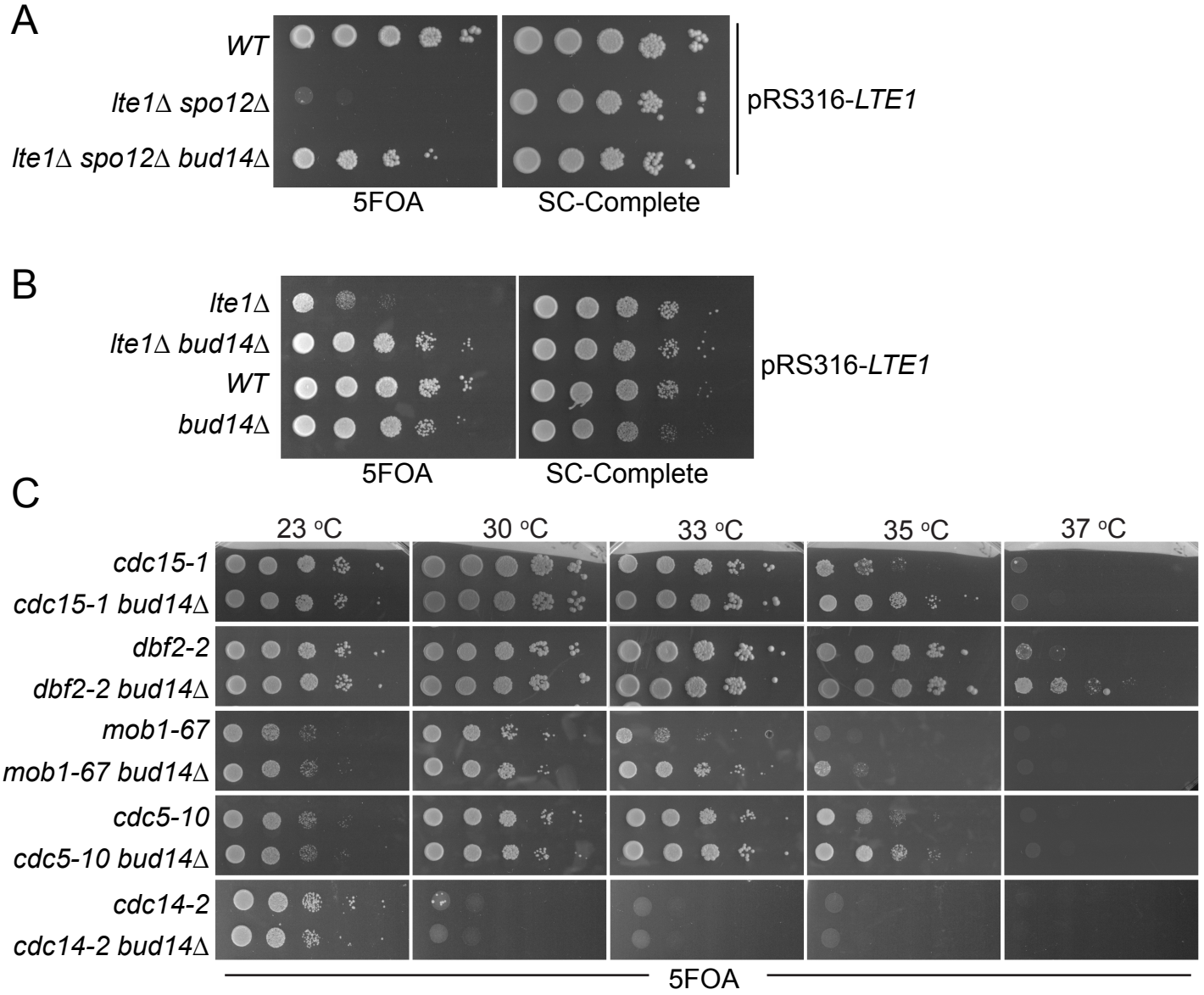
A
WT
lte1Δ spo12Δ
lte1Δ spo12Δ bud14Δ
pRS316-LTE1
5FOA
SC-Complete
B
lte1Δ
lte1Δ bud14Δ
WT
bud14Δ
pRS316-LTE1
5FOA
SC-Complete
C
23 °C
30 °C
33 °C
35 °C
37 °C
cdc15-1
cdc15-1 bud14Δ
dbf2-2
dbf2-2 bud14Δ
mob1-67
mob1-67 bud14Δ
cdc5-10
cdc5-10 bud14Δ
cdc14-2
cdc14-2 bud14Δ
5FOA

Figure 2

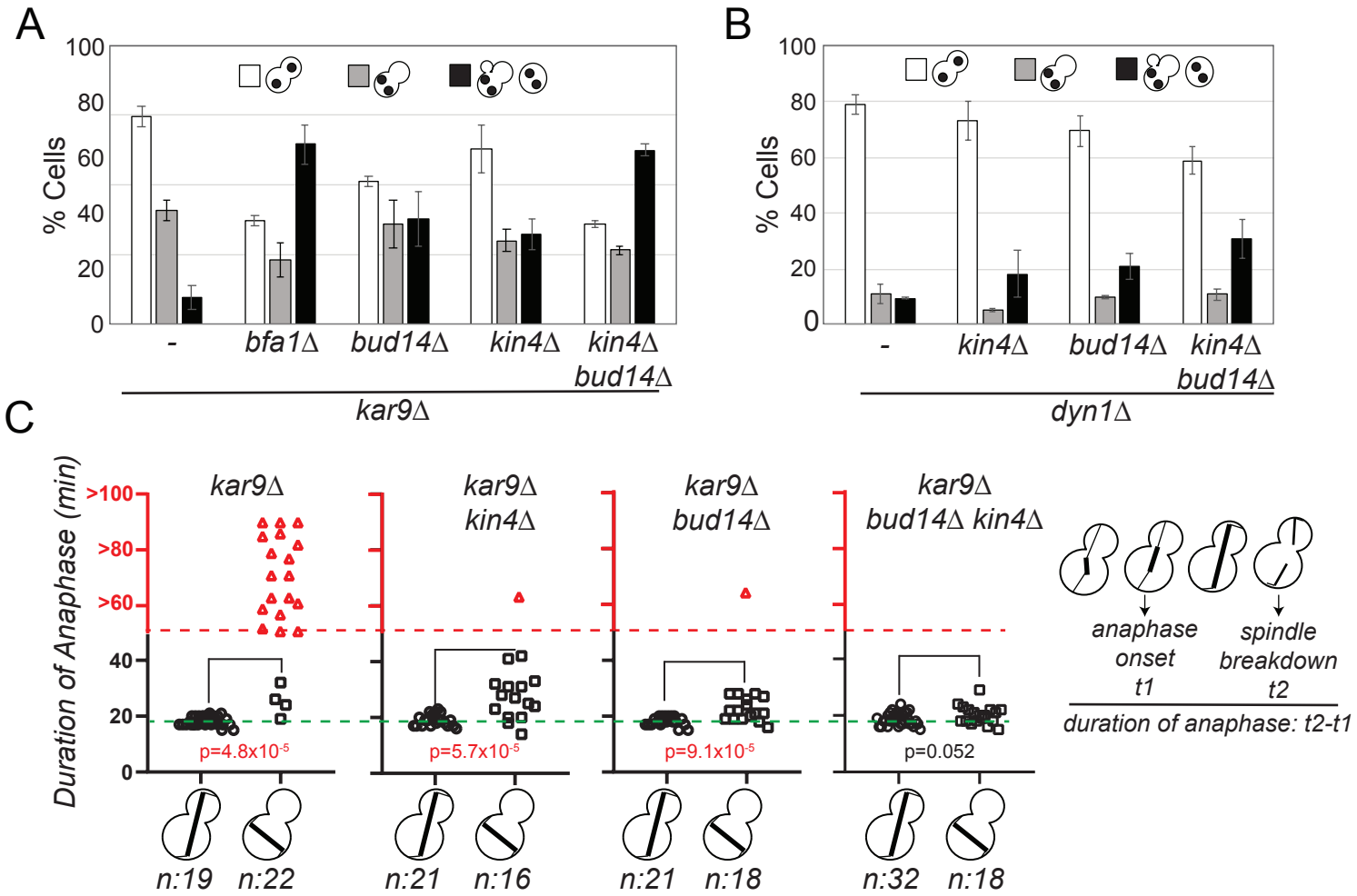
A
100
80
60
40
20
0
% Cells
-
bfa1Δ
bud14Δ
kin4Δ
kin4Δ bud14Δ
kar9Δ
B
100
80
60
40
20
0
% Cells
-
kin4Δ
bud14Δ
kin4Δ bud14Δ
dyn1Δ
C
Duration of Anaphase (min)
>100
>80
>60
40
20
0
kar9Δ
kar9Δ kin4Δ
kar9Δ bud14Δ
kar9Δ bud14Δ kin4Δ
p=4.8x10-5
p=5.7x10-5
p=9.1x10-5
p=0.052
n:19
n:22
n:21
n:16
n:21
n:18
n:32
n:18
anaphase onset t1
spindle breakdown t2
duration of anaphase: t2-t1

Figure 3

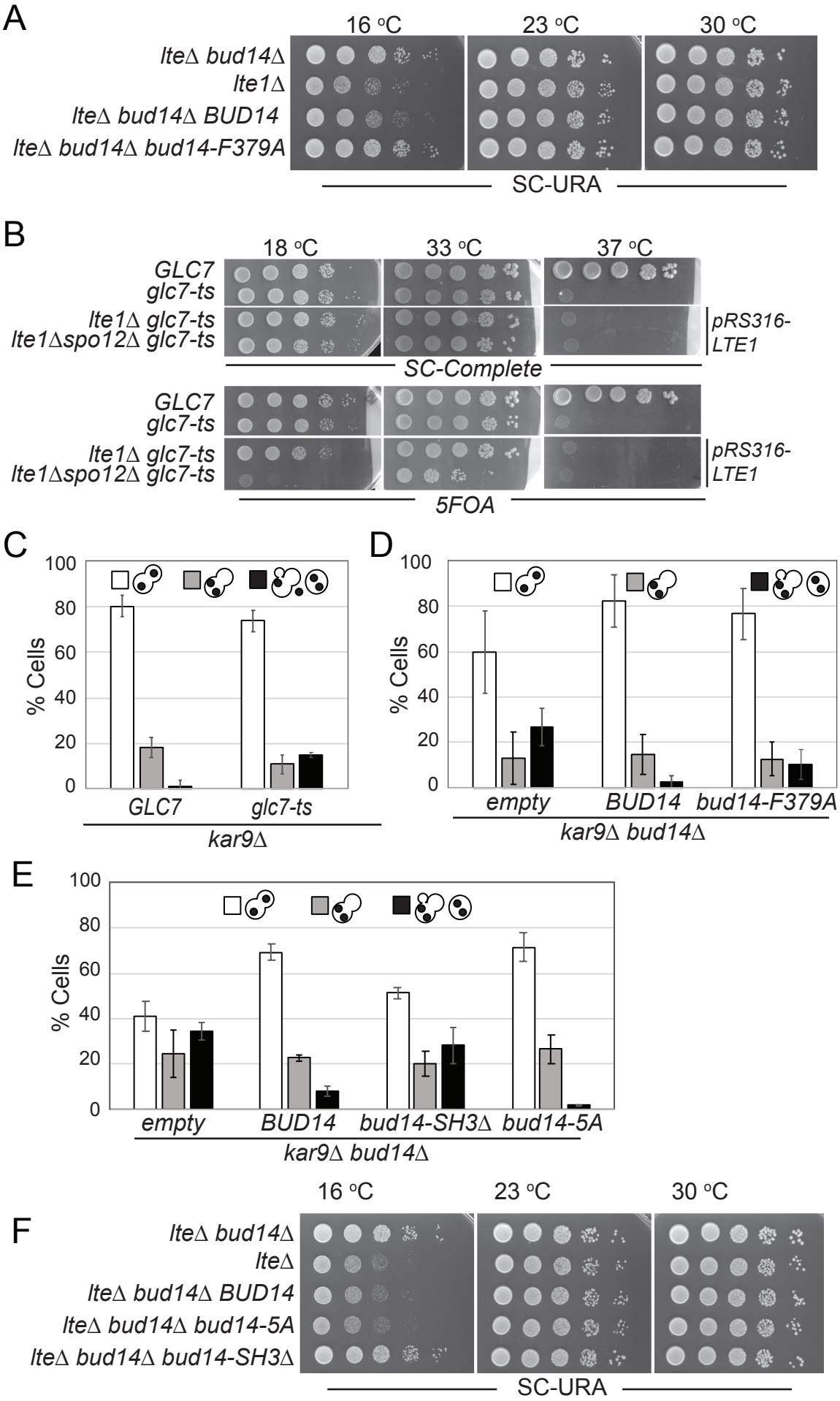
A
16 °C
23 °C
30 °C
lteΔ bud14Δ
lte1Δ
lteΔ bud14Δ BUD14
lteΔ bud14Δ bud14-F379A
SC-URA
B
18 °C
33 °C
37 °C
GLC7
glc7-ts
lte1Δ glc7-ts
lte1Δspo12Δ glc7-ts
pRS316-LTE1
SC-Complete
GLC7
glc7-ts
lte1Δ glc7-ts
lte1Δspo12Δ glc7-ts
pRS316-LTE1
5FOA
C
% Cells
100
80
60
40
20
0
GLC7
glc7-ts
kar9Δ
D
% Cells
100
80
60
40
20
0
empty
BUD14
bud14-F379A
kar9Δ bud14Δ
E
% Cells
100
80
60
40
20
0
empty
BUD14
bud14-SH3Δ
bud14-5A
kar9Δ bud14Δ
F
16 °C
23 °C
30 °C
lteΔ bud14Δ
lteΔ
lteΔ bud14Δ BUD14
lteΔ bud14Δ bud14-5A
lteΔ bud14Δ bud14-SH3Δ
SC-URA

Figure 4

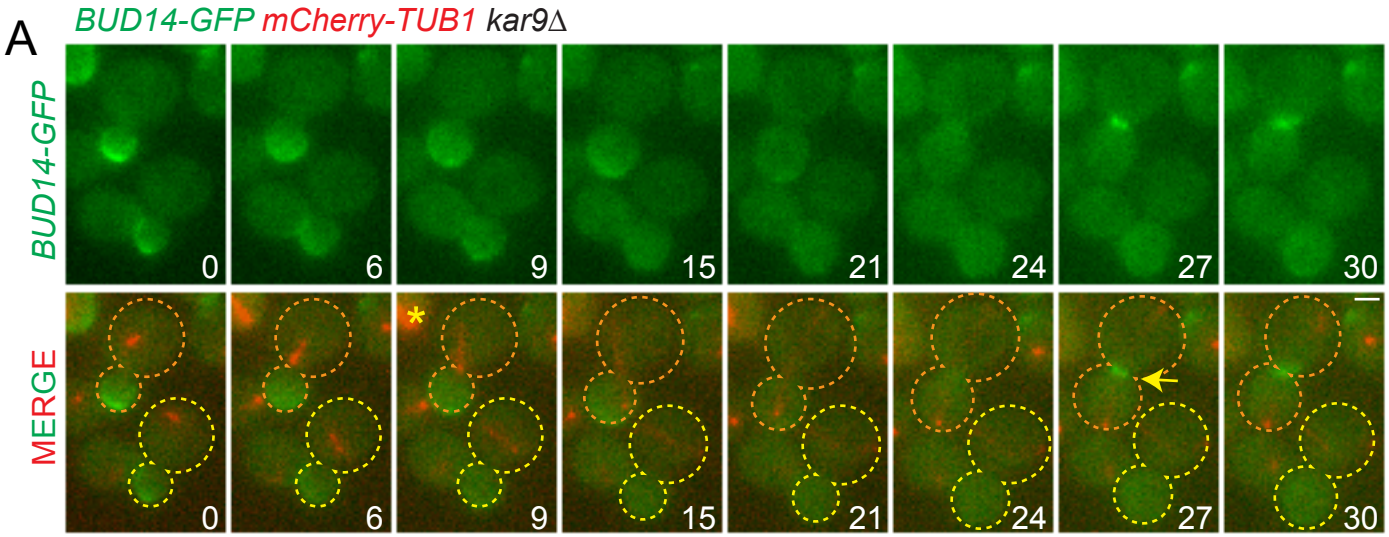
A
BUD14-GFP mCherry-TUB1 kar9Δ
BUD14-GFP
MERGE
0
6
9
15
21
24
27
30
*

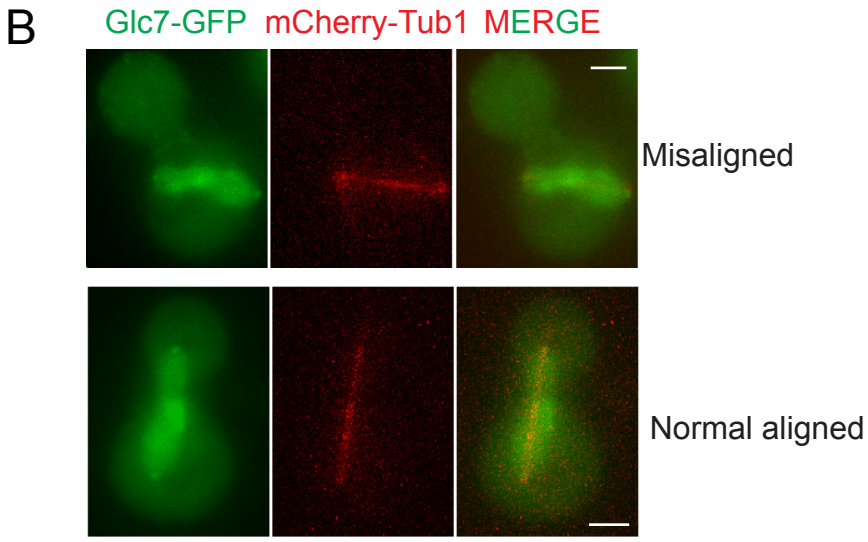
B
Glc7-GFP mCherry-Tub1 MERGE
Misaligned
Normal aligned

Figure 5

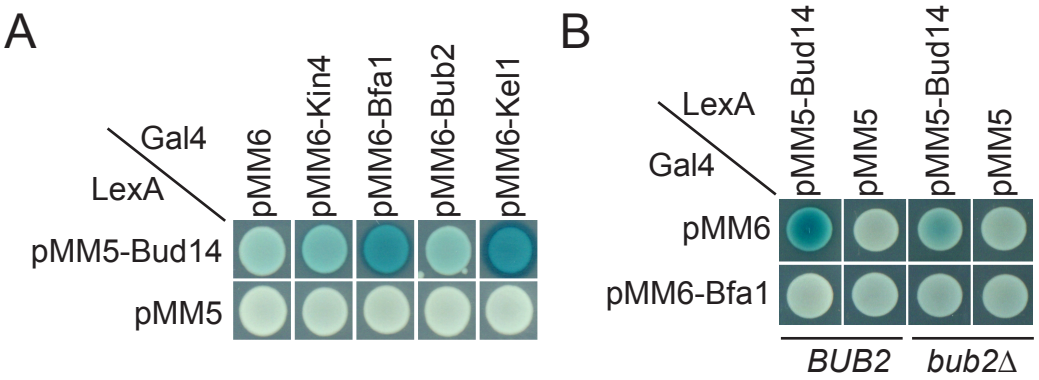
A
Gal4
LexA
pMM6
pMM6-Kin4
pMM6-Bfa1
pMM6-Bub2
pMM6-Kel1
pMM5-Bud14
pMM5
B
LexA
Gal4
pMM5-Bud14
pMM5
pMM5-Bud14
pMM5
pMM6
pMM6-Bfa1
BUB2
bub2Δ

Figure 6

A

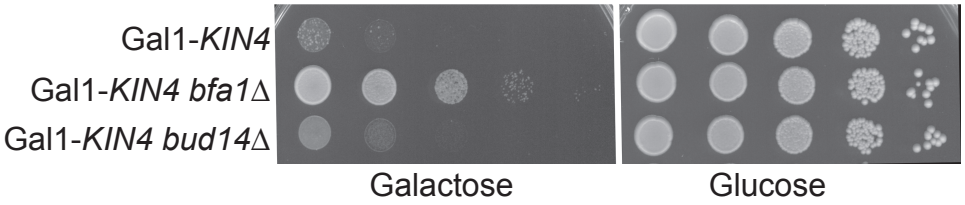

B

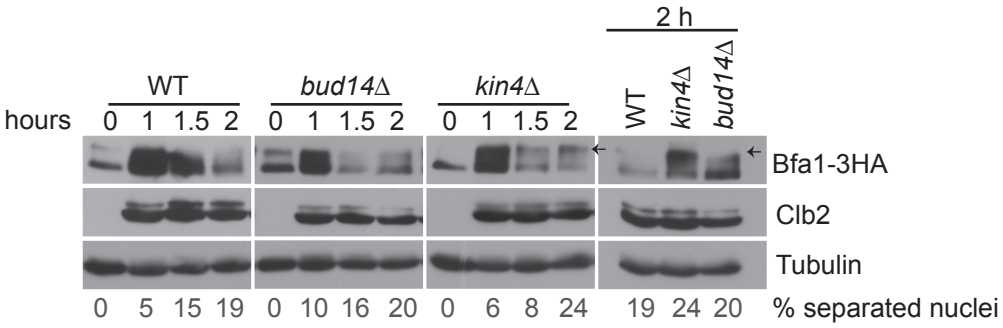

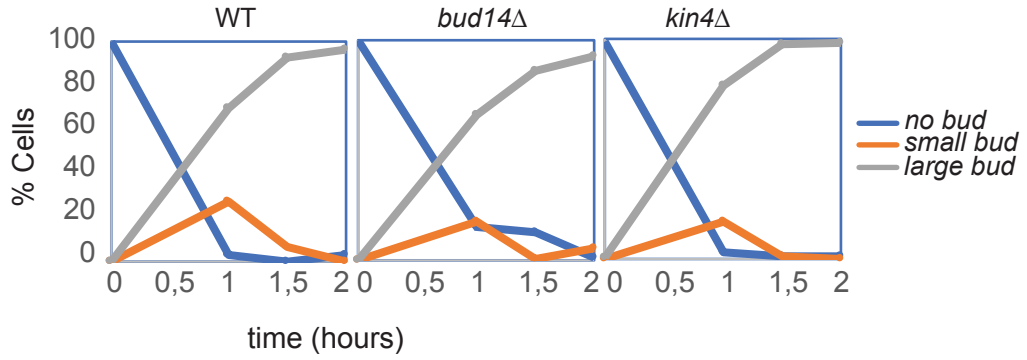

C

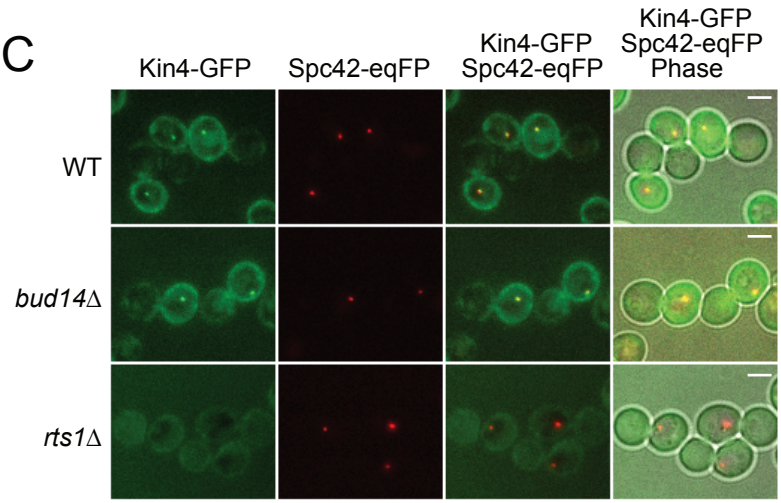

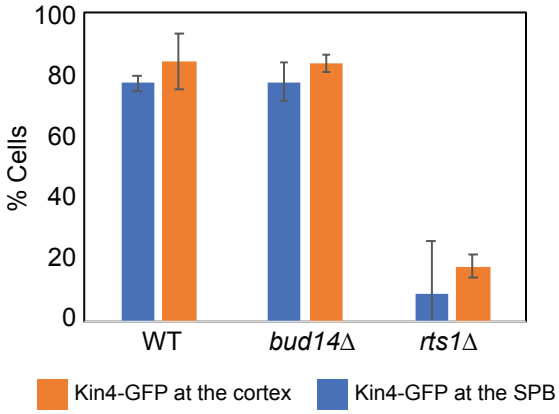

D

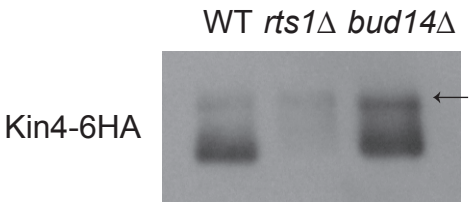

Figure 7

A

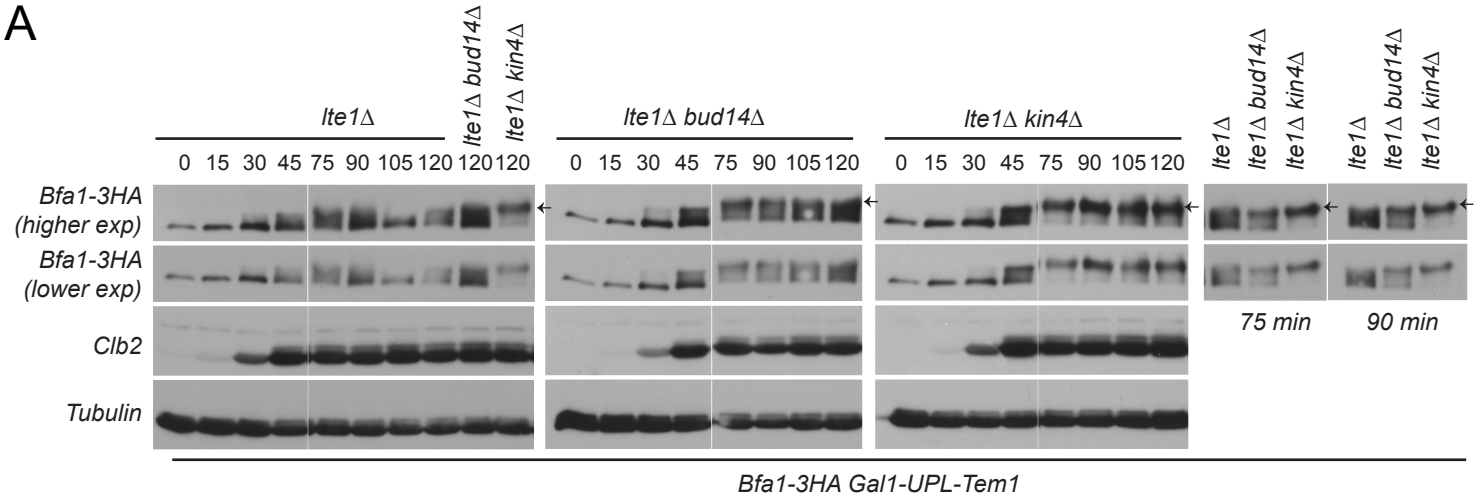

B

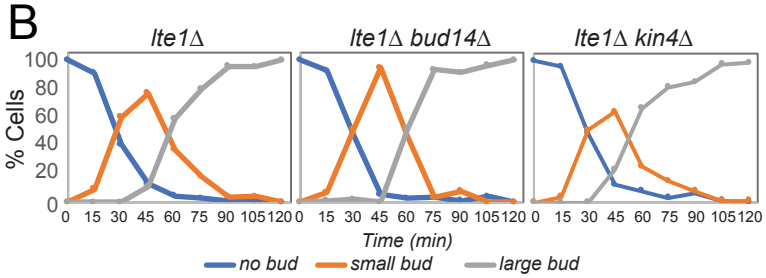

C

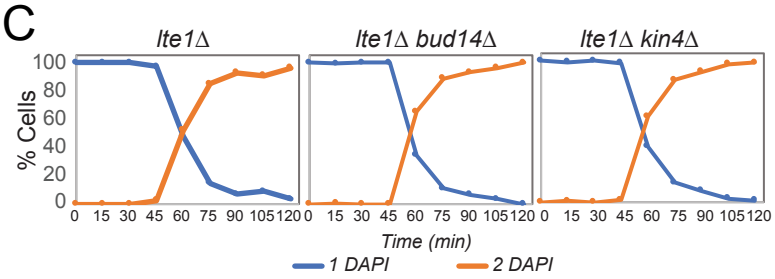

D

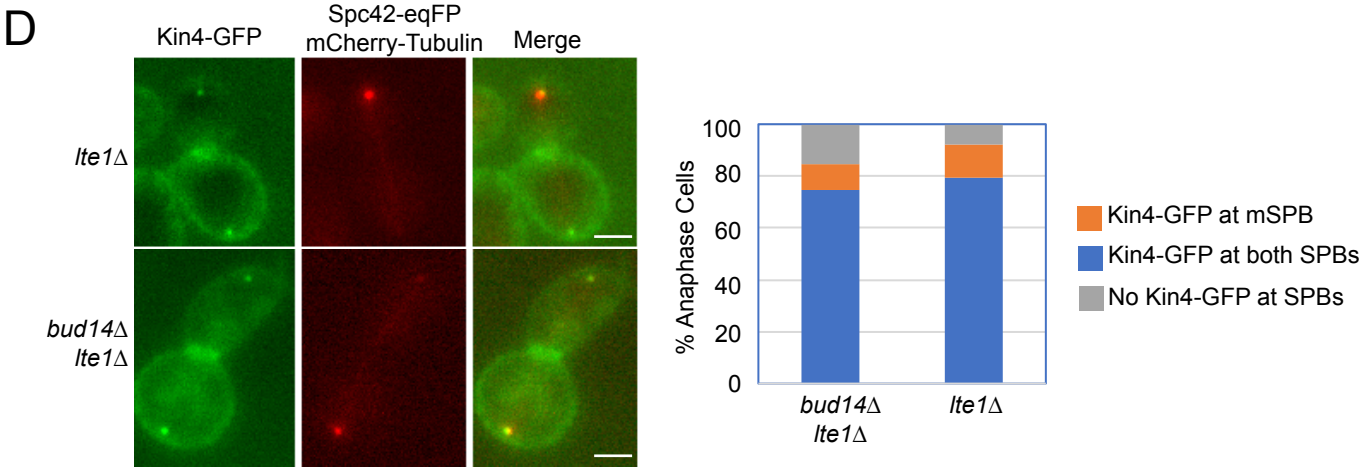

Figure 8

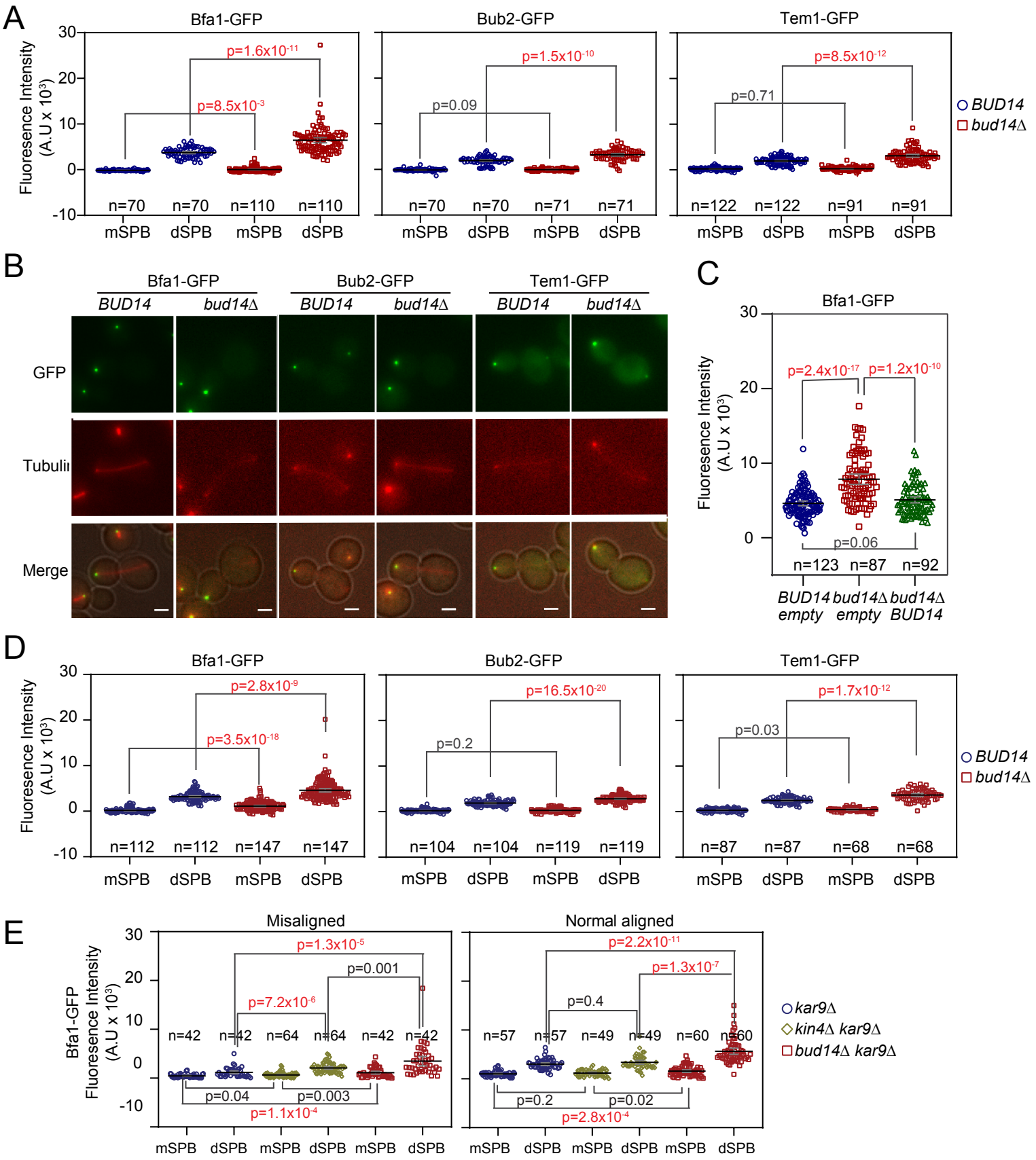
A
Bfa1-GFP
Bub2-GFP
Tem1-GFP
Fluoresence Intensity (A.U x 10³)
p=1.6x10-11
p=8.5x10-3
p=1.5x10-10
p=0.09
p=8.5x10-12
p=0.71
n=70 n=70 n=110 n=110
n=70 n=70 n=71 n=71
n=122 n=122 n=91 n=91
mSPB dSPB mSPB dSPB
BUD14
bud14Δ
B
Bfa1-GFP
Bub2-GFP
Tem1-GFP
BUD14
bud14Δ
GFP
Tubulin
Merge
C
Bfa1-GFP
Fluoresence Intensity (A.U x 10³)
p=2.4x10-17
p=1.2x10-10
p=0.06
n=123 n=87 n=92
BUD14 empty
bud14Δ empty
bud14Δ BUD14
D
Bfa1-GFP
Bub2-GFP
Tem1-GFP
Fluoresence Intensity (A.U x 10³)
p=2.8x10-9
p=3.5x10-18
p=16.5x10-20
p=0.2
p=1.7x10-12
p=0.03
n=112 n=112 n=147 n=147
n=104 n=104 n=119 n=119
n=87 n=87 n=68 n=68
mSPB dSPB mSPB dSPB
BUD14
bud14Δ
E
Misaligned
Normal aligned
Bfa1-GFP Fluoresence Intensity (A.U x 10³)
p=1.3x10-5
p=0.001
p=7.2x10-6
n=42 n=42 n=64 n=64 n=42 n=42
p=0.04
p=0.003
p=1.1x10-4
p=2.2x10-11
p=1.3x10-7
p=0.4
n=57 n=57 n=49 n=49 n=60 n=60
p=0.2
p=0.02
p=2.8x10-4
mSPB dSPB mSPB dSPB mSPB dSPB
kar9Δ
kin4Δ kar9Δ
bud14Δ kar9Δ

Figure 9

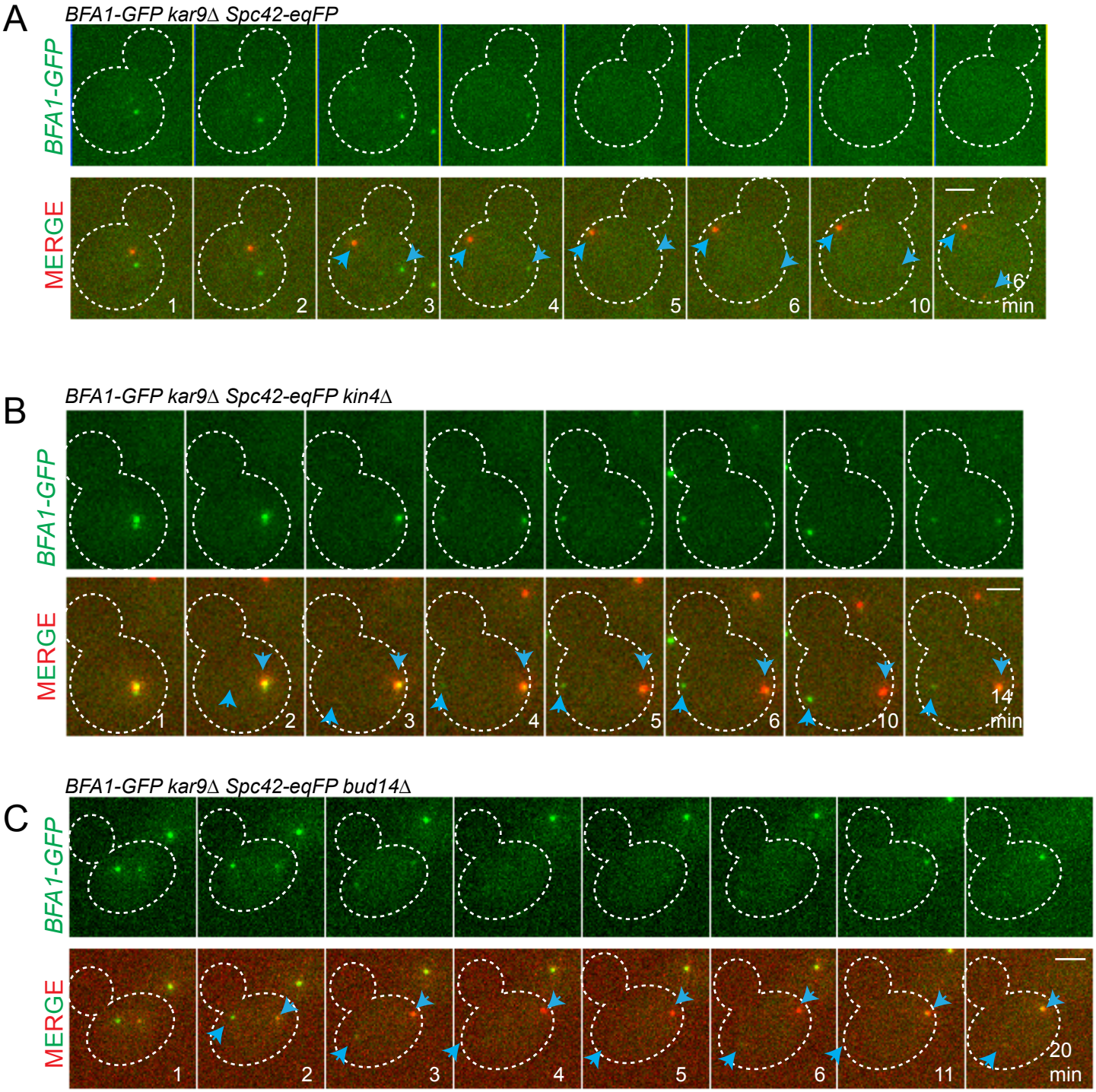
A
BFA1-GFP kar9Δ Spc42-eqFP
BFA1-GFP
MERGE
1
2
3
4
5
6
10
16 min
B
BFA1-GFP kar9Δ Spc42-eqFP kin4Δ
BFA1-GFP
MERGE
1
2
3
4
5
6
10
14 min
C
BFA1-GFP kar9Δ Spc42-eqFP bud14Δ
BFA1-GFP
MERGE
1
2
3
4
5
6
11
20 min